C.P. No. 1052

C.P. No. 1052

MINISTRY OF TECHNOLOGY

AERONAUTICAL RESEARCH COUNCIL

CURRENT PAPERS

Free Flight Measurements of the Longitudinal Stability of a Transonic Swept-Winged Aircraft

by

G. K. Hunt

Structures Dept., R.A.E., Farnborough

LONDON. HER MAJESTY'S STATIONERY OFFICE

1969

THIRTEEN SHILLINGS NET

U.D.C. 533.6.055 : 533.6.013.412 : 629.137.1 :
533.6.011.35 : 533.693.1

C.P. No.1052*
July 1968

FREE FLIGHT MODEL MEASUREMENTS OF THE LONGITUDINAL STABILITY OF A TRANSONIC SWEPT-WINGED AIRCRAFT

by

G. K. Hunt

SUMMARY

Four models of an aircraft configuration with a 55 degree swept wing were flown at Mach numbers between 0.9 and 1.4, at Reynolds numbers up to 10 million and lift coefficients between zero and 0.5. Measurements of the manoeuvre margin and the derivatives m_w, $(m_q + m_{\dot{w}})$ and z_w were obtained.

The results are compared with those obtained from one of the same models in a transonic wind tunnel and from a related M-wing model in flight. They are also corrected for aeroelastic effects.

---

* Replaces R.A.E. Technical Report 68178 - A.R.C. 31021.

CONTENTS

		Page
1	INTRODUCTION	3
2	MODEL DESIGN	4
	2.1 Geometry	4
	2.2 Construction	6
3	EXPERIMENTAL TECHNIQUE	6
	3.1 Stiffness measurements	6
	3.2 Wind-tunnel tests	6
	3.3 Free-flight tests	7
4	ANALYSIS AND PRESENTATION OF DATA	8
	4.1 Free-flight measurements	8
	4.2 Wind-tunnel measurements, and tunnel/flight comparison	10
	4.3 Comparison with M-wing model	12
	4.4 Aeroelastic effects	13
5	UNCERTAINTY OF THE FLIGHT TEST DATA	13
6	DISCUSSION OF RESULTS	14
7	CONCLUSIONS	17
Appendix A	Model geometry	19
Appendix B	Aeroelastic corrections	23
Appendix C	Model weight and inertia characteristics	27
Symbols		28
References		31
Illustrations		Figures 1-27
Detachable abstract cards		-

1 INTRODUCTION

About twelve years ago, a considerable research effort was directed towards the establishment of design principles for the first supersonic transport aircraft. Two classes of aircraft were considered: the slender delta, with an optimum performance at a Mach number of 2 or more; and the transonic swept-winged aircraft, which would cruise at low supersonic Mach numbers and would depend for its economic operation on the maintenance of a shock-free subsonic type of flow on the wing.

The work on swept-winged aircraft included a series of free-flight model tests of a wing-body combination suitable for a transport aircraft to cruise at a Mach number of 1.2. The primary purposes for which the models were flown were the investigation of methods of wing design and body design, and the measurement of engine nacelle installation drag. For these experiments, it was necessary to trim and manoeuvre the models in flight and accordingly they were all equipped with tails.

A preliminary model was flown to prove the model design. It was disturbed by pulse rockets at regular intervals throughout its flight, so that its stability could be measured. It yielded only a few measurements, but it served its purpose and no other models were flown specifically to obtain stability data. However, three of the other models were disturbed regularly in pitch by rapid movements of their tailplanes. Although they were flown for different purposes they carried sufficient instruments to enable their responses to the disturbances to be analysed. Hence a number of free-flight measurements of longitudinal stability were available as a bonus from other experiments. These experiments took several years to complete, because their pace was reduced drastically when the slender wing was chosen for the first supersonic transport. Now the flight records have been analysed to obtain the manoeuvre margin and the derivatives m_w, $(m_q + m_{\dot{w}})$ and z_w.

Before they were flown, two of the models were tested in a transonic wind tunnel, to provide information which would aid in planning the free-flight experiments and ensure that the models were trimmed and manoeuvred to greatest effect. The forces and moments on one of the models were measured, with and without a tail, over the range of Mach numbers covered by the flight tests. Hence the static lift and pitching-moment derivatives, and the manoeuvre margin, were determined.

The measurements of longitudinal stability, obtained in free flight and in the tunnel, have some shortcomings because they were not planned. They are incomplete, and would be of greater value if, for example, they included some free-flight measurements from a tailless model. They are affected by the small differences in geometry between the individual models, though fortunately the effects of these differences are generally either identifiable or negligible. In spite of these strictures, the measurements are of interest, not only in themselves but because they afford an opportunity to make a comparison between the results of two different experimental techniques.

Corrections have been applied to the manoeuvre margin and the static derivatives m_w and z_w, to allow for aeroelasticity. They are based on experimental measurements of the stiffness characteristics of the wings and estimates of those of the body and tail. They show that aeroelastic effects are significant, even on models with solid steel wings, and should not be ignored.

In parallel with the swept-wing experiments, a programme of work on M-wings was in progress. Dynamic longitudinal stability measurements were obtained in free flight from an M-wing model which had the same gross wing area as the swept-wing models and a similar body and tail. Comparison of the results from the swept-wing and M-wing models indicates some of the essential differences between the characteristics of the two kinds of aircraft shape.

2 MODEL DESIGN

2.1 Geometry

The models (Fig.1) represented a swept-wing-body combination of the kind shown by Bagley[1] to be suitable for a transonic transport aircraft. All the models had a tail to provide stability and control, but this was designed to suit the requirements of the free-flight experiments and not to represent a possible aircraft tail.

The models were based as far as possible on Bagley's proposals, and the wing planform was the one that he suggested. The wing was swept back 55 degrees and had a gross aspect ratio of 3.40. The trailing edge was straight from root to tip, with a constant chord over the inboard half of the span and a parabolic leading edge on the outboard half that reduced the chord to zero at the tip. The aerofoil section was RAE 101 with a uniform thickness/chord ratio of 0.06. This made the wing twice as thick as that of the aircraft proposed by Bagley, but it was necessary to provide enough strength to allow the models to be manoeuvred at low altitude.

The stability measurements were obtained from models with two different body profiles, because one of the original purposes of the experiments had been to investigate methods of body design[2]. Model 1 had a body of revolution consisting of a von Karman ogive nose, a cylindrical centre part, and an afterbody with the same profile as the nose but cut off to form a finite base (Fig.2). Models 2, 3 and 4, which provided most of the stability measurements, had a body of revolution designed by redistributing the volume of this basic ogive-cylinder-ogive in a manner determined by the area rule for a design Mach number of 1.16 (Figs.2 and 3). The cross-section areas of this body differed from those of the basic body by only 60 per cent of the amounts required by the area rule. This procedure was justified by calculations by Lord[3], and measurements made in free flight[2] showed that the flow in the wing-body junction remained shock-free up to $M = 1.4$ at zero lift.

Each model was equipped with a cylindrical probe with a hemispherical tip, $\frac{1}{2}$ inch in diameter, which extended forward along the body axis from the nose (Figs.1 and 3). Models 2, 3 and 4 carried a cone-cylinder fairing under the tail (Figs.1 and 3) which contained a pyrotechnic flare to facilitate visual tracking from the ground.

The tail unit was designed to suit model engineering requirements. The tailplane had a planform with good structural properties and an orderly movement of its aerodynamic centre position throughout the transonic speed range. The tailplane was mounted on top of the fin so that, when it was required for use as a pitch control, adequate hinge moments could be produced by a small actuator in the body driving a long lever inside the fin. The tailplane section was RAE 101, with a uniform thickness/chord ratio of 0.04, and the fin section was hexagonal.

On Model 1 the tailplane was fixed parallel to the body axis. On Models 2, 3 and 4 the tailplane was pivoted about an axis near the top of the fin, and there were gaps below the tailplane to allow it to move (Fig.3). Stops were provided to limit the tailplane movement between angles of approximately -6 degrees and zero, measured relative to the body axis.

Every model except No.4 had a plane, unwarped wing mounted symmetrically in the body at zero incidence. The wing of Model 4 was cambered and twisted[4] with the object of producing, at a Mach number of 1.2 and a design C_L of 0.15, a uniform distribution of C_L across the span and a prescribed trapezoidal chordwise load distribution (Fig.4). This wing was twisted about its

trailing edge, which thus remained straight. The wing was mounted in the body at its calculated zero-lift angle, with the trailing edge intersecting the body centre line (Fig.3). Median lines of sections through the wing are plotted in Fig.5.

Ordinates of the wing planform and of the body profiles, and the ranges of movement of the individual tailplanes of Models 2, 3 and 4 are given in Appendix A.

2.2 Construction

The body of each model was made from four hollow castings of aluminium alloy, with walls about $\frac{1}{4}$ inch thick. Particular care was taken during design and manufacture to prevent movement at the joints under the loads imposed in flight. The wings of Model 1 were made from laminations of aluminium-alloy plate, bonded together and built up to the correct profile with epoxy resin. The wings of Models 2, 3 and 4 were made of solid steel because they were more heavily loaded in flight. All the tailplanes were made from solid aluminium alloy.

The ordinates of all external profiles were held within a dimensional tolerance of ±0.003 inch.

3 EXPERIMENTAL TECHNIQUE

3.1 Stiffness measurements

To enable the effects of aeroelastic distortion to be calculated, the stiffness characteristics of a laminated and a solid wing were measured. The stiffness characteristics of the body and tail were estimated. The losses of lift and pitching moment due to aeroelasticity were then calculated iteratively.

The methods used to determine stiffness and to calculate the effects of aeroelasticity on the static stability derivatives and the manoeuvre margin are described in detail in Appendix B.

3.2 Wind-tunnel tests

Two of the free-flight models were tested, before being flown, in the A.R.A. 9ft × 8ft transonic wind tunnel. The tests covered the range of Mach numbers from 0.7 to 1.4, at Reynolds numbers of about 4×10^6.

Model 3 was tested without its tail, to obtain direct measurements of the downwash at the tailplane position (Fig.19). Measurements of lift, drag and pitching moment were obtained from Model 4, with and without its tail, and

these measurements were analysed to find the mean downwash at the tail. This work is described by Haines and Jones[5]. The static stability derivatives were determined from the force and moment measurements for the purpose of the present report (see section 4.2).

The models were modified for these tests so that they could be supported on a sting (Fig.19). The tail of Model 3 was removed and the afterbody replaced by a shorter one with reduced surface slopes. The afterbody of Model 4 was replaced by a cylinder of the same length and a shorter fin was fitted so that the distance from the tailplane to the body axis would be unchanged.

3.3 Free-flight tests

When each model was ready to fly, its weight, centre of gravity position and moments of inertia were measured. These characteristics are tabulated in Appendix C. The moments of inertia were measured about the body axis and about spanwise and normal axes through the centre of gravity, by suspending the model on a single wire and swinging it as a torsional pendulum about each axis in turn.

The models were launched from the ground and reached their maximum velocity in about 3 seconds (Fig.6). They all achieved maximum Mach numbers near 1.45 and maximum Reynolds numbers, based on $\bar{\bar{c}}$, of about 10 million (Fig.7). The booster rockets (Fig.3) were detached as soon as they stopped thrusting, and the experimental measurements were made while the models were decelerating in free flight. Boundary-layer transition was allowed to occur naturally.

Model 1 was disturbed at intervals of about 1.5 seconds by firing single-shot pulse rockets, fixed in the body, in a direction normal to the plane of the wing. The ports in the body through which they were fired are shown in Fig.3. Models 2, 3 and 4 were disturbed at intervals of about 1 second by rotating the tailplane quickly between the fixed stops. The tailplane always completed its movement in less than 0.010 second. This interval is an order of magnitude smaller than the period of the longitudinal motion of the models and allows the change of angle of the tailplane to be regarded as a step.

Model 1 was trimmed to fly at zero lift, but the trim of Models 2, 3 and 4 was changed by each movement of the tailplane. With the tailplane against one stop the models were trimmed at zero lift, but against the other stop they

were trimmed at lift coefficients which ranged, at supersonic speeds, between 0.2 and 0.5 (Fig.8). Thus for half the time that they were in the air Models 2, 3 and 4 flew with a mean normal acceleration of about 15 g. As a precaution to prevent them straying beyond the safety limits of the range, these three models were built with a differential angle of incidence of $\frac{1}{4}$ degree between the port and starboard wings. This forced them to roll continuously in flight (Fig.9) and thus to perform a barrel roll about a ballistic trajectory (Fig.10). The effect of the steady rate of roll on the responses of the models to disturbances is discussed in section 4. Every model carried standard R.A.E. 465 MHz telemetry equipment which provided measurements of normal acceleration at the nose, centre of gravity and tail, and of lateral acceleration at the centre of gravity. The flight-path coordinates and velocity of each model were determined from observations made by synchronised kinetheodolites at several stations on the ground. Additional measurements of velocity were obtained by means of a radio-Doppler system. Ambient pressure and local static temperature were determined from radio-sonde measurements.

4 ANALYSIS AND PRESENTATION OF DATA

4.1 Free-flight measurements

The method used to analyse the flight records was developed by H.M.A. Voepel, specifically to suit free-flight experiments in which all information about the responses of the models to disturbances is obtained from linear accelerometers. It depends on three assumptions. The longitudinal motion is assumed to be unaffected by any lateral motion, and the degrees of freedom in roll, yaw and sideslip are ignored. It is also assumed that the aerodynamic derivatives, and thus the Mach number, remain constant for the duration of each response. This allows the motion to be regarded as having only two degrees of freedom. The third assumption is that the pitching and heaving components of the motion are in phase, and that there is thus a centre of rotation ahead of the centre of gravity about which the model oscillates (the so-called focal point). The aerodynamic derivatives are then related to the frequency and damping of the longitudinal short-period oscillation and the distance from the centre of gravity to the focal point. The analysis is set out in full in Ref.6 and leads to the following expressions for the derivatives and the manoeuvre margin:

$$m_w = -\frac{i_B}{\mu_1}(\omega_{n1}\,\hat{t})^2 \qquad (1)$$

$$z_w = -\frac{\hat{t}}{V}\omega_{n1}^2\,D_1 \qquad (2)$$

$$(m_q + m_{\dot{w}}) = -i_B\,(z_w + 2\hat{t}\,\lambda_1) \qquad (3)$$

$$H_m = \frac{i_B\,\bar{c}}{D_1} \quad . \qquad (4)$$

The pitching axis to which the manoeuvre margin and the moment derivatives relate, when calculated by means of these equations, passes through the centre of gravity.

Two examples of flight records are shown in Fig.11. The first is from Model 1 and shows the responses to the sequence of pulse-rocket disturbances. The rockets were offset slightly from the model centre line (Fig.3) and most of them disturbed the model laterally as well as longitudinally. The resultant motion was a combination of the longitudinal short-period oscillation and the Dutch roll, with sufficient cross-coupling between the two modes to invalidate seperate analysis of the longitudinal motion. Fortunately, three of the pulse rockets excited a pure longitudinal motion that could be analysed. The second record is from Model 3. The oscillations took place alternately about the two trimmed conditions associated with the limiting tailplane angles. There was always a slight lateral response to the tailplane movements, probably caused by inertia coupling between the steady rate of roll and the high initial rates of pitch after the sudden movements of the control. Nevertheless the lateral amplitude was always small compared to the longitudinal amplitude, and eleven of the longitudinal responses of this model were analysed satisfactorily.

The steady rate of roll that was imposed on Models 2, 3 and 4 had a negligible effect on their longitudinal stability. Calculation shows that, at the design Mach number of 1.2, a rate of roll of 150 deg/sec reduces the longitudinal short-period frequency by less than one-fifth of one per cent.

The frequency and damping of the longitudinal short-period oscillation are plotted in Figs.12 and 13, and the reduced undamped frequency in Fig.14. The stability derivatives are plotted in Figs.15-18. Since the centre of gravity positions of all the models differed from each other, the values of m_w and H_m have been adjusted to relate to a common pitch axis position at the aerodynamic mean quarter-chord point. The adjusted values were obtained from the measured values by means of the relationships:

$$m_{w_A} = m_{w_M} + \frac{\Delta x}{\bar{c}} z_w \tag{5}$$

$$H_{m_A} = H_{m_M} + \frac{\Delta x}{\bar{c}} \quad . \tag{6}$$

The appropriate experimental values of z_w were used in equation (5). The measurements of $(m_q + m_{\dot{w}})$ were not adjusted and each value relates to the centre of gravity position of the model from which it was obtained.

4.2 Wind-tunnel measurements, and tunnel/flight comparison

The modifications to Models 3 and 4 to allow them to be tested in the A.R.A. transonic wind tunnel are shown in Fig.19. In Fig.20 the free-flight measurements are compared with unpublished measurements obtained in the tunnel from Model 4 with its tail on.

Since the free-flight tests were intended to provide information about the wing-body combination, the contributions from the tail to the derivatives m_w and z_w were estimated. These contributions were calculated by means of the expressions

$$\Delta m_w = \frac{l_T}{\bar{c}} z_{w_T} \frac{S_T}{S}\left(1 - \frac{\partial \varepsilon}{\partial \alpha}\right) \tag{7}$$

$$\Delta z_w = z_{w_T} \frac{S_T}{S}\left(1 - \frac{\partial \varepsilon}{\partial \alpha}\right) \quad . \tag{8}$$

The lift-curve slope and aerodynamic centre position of the tailplane were found from the charts and tables of Stanbrook[7] and Smith, Beasley and Stevens[8], which are all based on linear theory. Exact calculation of the downwash at the tail was not attempted, but instead an arbitrary value of 0.3 was assumed for $\partial\varepsilon/\partial\alpha$ at all Mach numbers. A good indication of the errors introduced by making this assumption is given by Fig.21, which reproduces Haines' and Jones' curves[5] of $\partial\varepsilon/\partial\alpha$ at the tailplane position in the tunnel. The downwash at the tail of Model 3 was measured at the points shown in Fig.19a, and the downwash at the tail of Model 4 was obtained by an analysis of the measurements of lift and pitching moment on the model with and without its tail. The estimated contributions from the tail to m_w and z_w are plotted in Fig.22, before and after making allowance for aeroelastic effects on the body and tailplane (see Appendix B). The contributions from the tail that were measured in the

tunnel, in the form of the difference between the tail-off and tail-on measurements, are plotted in the same figure for comparison. The estimated contributions from the tail, corrected for aeroelasticity, were subtracted from the free-flight measurements to obtain curves for the wing-body combination. These are plotted in Fig.23, where they are compared with the tunnel curves for Model 4 without its tail.

Values of m_w and z_w were obtained from the wind-tunnel measurements by finding the slopes of the curves of lift and pitching moment, plotted either against each other or against angle of attack. The slopes were measured at zero lift and at the mean of the high lift coefficients measured in free flight at the same Mach number. Then

$$m_w = \frac{1}{2}\frac{\partial C_m}{\partial \alpha} = \frac{1}{2}\frac{\partial C_m}{\partial C_L}\frac{\partial C_L}{\partial \alpha} \qquad (9)$$

and

$$z_w = -\frac{1}{2}\left(\frac{\partial C_L}{\partial \alpha} + C_D\right) \simeq -\frac{1}{2}\frac{\partial C_L}{\partial \alpha} \quad . \qquad (10)$$

The values of m_w obtained from equation (9) were adjusted to relate to a pitch axis at $\bar{c}/4$ by means of equation (5).

The free-flight tests yielded the true manoeuvre margin, given by

$$H_m = \frac{m_w}{z_w} - \frac{m_q}{\mu_1} \qquad (11)$$

and this is the quantity plotted for the complete models in Figs.17, 20c, 23c and 25. However m_q was not measured in the tunnel, and the contribution to m_q from the tail could not be estimated reliably. Hence the curves in Fig.20c for the model in the tunnel, and in Fig.23c for the wing-body combination, show the static margin given by

$$H_n = \frac{m_w}{z_w} \qquad (12)$$

because this was all that could be calculated from the data available. Nevertheless they are presented as curves of manoeuvre margin because the error introduced by omitting the m_q term is about 0.003, which is trivial.

No attempt has been made to estimate $(m_q + m_{\dot{w}})$ for the tailless configuration. Approximate estimates of the contribution to the rotary derivatives from the tail, based on the concept of delayed downwash, are

unreliable for tails behind swept wings at transonic speeds. Thomas' and Spencer's exact method[9] applies to swept wings at subsonic speeds only, and thus has practically no application in this case.

4.3 Comparison with M-wing model

At the same time as the work on swept wings was being done, other free-flight experiments were in progress to measure the drag and longitudinal stability of a closely related M-wing configuration. The M-wing is based on the same design principles as the swept wing. In Ref.1, Bagley proposed an M planform as an alternative to the swept wing, and this was adopted for the free-flight models. In as many other respects as possible the M-wing models resembled the swept-wing models because it was intended that the measurements obtained from the two kinds of model should be directly comparable[10].

Stability measurements were obtained from the M-wing model shown in Fig.24. It had the same gross wing area, the same sweep angle, the same aerofoil section and the same thickness/chord ratio as the swept-wing models. Its tail surfaces had the same planforms, and its body had the same length and slenderness ratio, as those of the swept-wing models. Apart from the wing planform, the M-wing model differed from the swept-winged models in that its body was a simple ogive-cylinder and its tailplane was a flat plate with chamfered edges.

The two sets of stability measurements are plotted together in Fig.25. The m_w and H_m measurements have been adjusted to relate to a pitch axis position at $\bar{\bar{c}}/4$, but it should be noted that the $\bar{\bar{c}}/4$ point of the M-wing was 2.226 inches, or roughly 0.2 $\bar{\bar{c}}$, nearer the nose than that of the swept-winged models. Because of this error in design, the body and tail contributions to the pitching-moment derivatives must be different for the two types of model.

The comparison in this Report between the longitudinal stability derivatives of the M-wing and swept-wing models supersedes that made by Edwards[10], which was based on an incomplete analysis of the tests on the swept wing. It confirms Edwards' finding that the transonic shift of the aerodynamic centre of the M-wing design is about half that of the swept-wing models (Fig.25c) but the two configurations are now shown to have virtually the same lift-curve slope (Fig.25a) in spite of the higher aspect ratio of the M wing. The difference in damping-in-pitch between the two kinds of model must be related to the difference

in tail arm as well as to the difference in wing planform. The tail arm of the M-wing model, measured from the model centre of gravity, was about 10 per cent greater than the tail arms of the swept-wing models.

The drag characteristics of the swept-wing and M-wing free-flight models are compared in Ref.11.

4.4 Aeroelastic effects

The loading lines assumed for the purpose of estimating the aeroelastic effects on the wing are shown in Fig.26, and the measurements of wing stiffness in Fig.27. The methods of calculating the effects of aeroelastic distortion of the wing, and of the body and tail, are described in Appendix B. The appropriate corrections to the experimental results are plotted in Figs.15, 16 and 17. Since the corrections for wing distortion were calculated specifically for the conditions prevailing at $M \approx 1.2$, only short lengths of the corrected curves have been drawn. Nevertheless the corrections for $M = 1.2$ are good approximations to the corrections required at all supersonic Mach numbers (see Appendix B).

5 UNCERTAINTY OF THE FLIGHT TEST DATA

The ambient conditions were determined with negligible error. The uncertainty in the velocity measurements arose almost entirely from the correction for wind velocity, and was about ±10 ft/sec. The resultant uncertainty in Mach number was therefore about ±0.01.

The uncertainty of the stability measurements has been analysed in detail by Picken[12]. Most of the uncertainty in the experimental values of m_w and z_w is due to the uncertainty of measurement of the longitudinal short-period frequency. This was about ±2 per cent, and the resultant uncertainty in m_w is about ±4 per cent, and in z_w about ±5 per cent. The uncertainty of the manoeuvre margin is the uncertainty of measurement of the focal-point position, and is about ±5 per cent in this case. The damping of the short-period oscillation was measured to within about ±10 per cent, and the resultant uncertainty in $(m_q + m_{\dot{w}})$ is about ±20 per cent.

These uncertainties apply to measurements made when the derivatives are not changing rapidly with Mach number. The greater the rates of change of the derivatives with Mach number, the more seriously the basic assumptions of the analysis are violated and the greater the uncertainty. Thus at near-sonic speeds, where the measurements are more scattered than at other Mach numbers, the uncertainties are probably greater than the figures given above.

6 DISCUSSION OF RESULTS

The telemetry equipment used in the flight experiments was a time-sharing system that transmitted brief samples of information from each accelerometer in turn at regular intervals. (In Fig.11 each dot is one sample.) Hence the best definition of a flight oscillation on the records was obtained when the oscillation frequency was low. The analysis of the flight records, both for the extraction of stability derivatives and for the other purposes for which the models were flown, was based on the assumption that the Mach number was constant. Since the Mach number fell continuously throughout every flight, the analysis of each response was confined to as short an interval of flight time as possible, so that the change of Mach number in that interval would be small. Thus the analysis was most likely to yield correct results when the oscillation frequency was high.

To strike a balance between these conflicting requirements the models were flown with their centres of gravity between 10 and 20 per cent further forward, in terms of $\bar{\bar{c}}$, than would be suitable for the corresponding full-scale aircraft. This reduced the uncertainty of the analysis and raised the reduced undamped frequency to a level more appropriate to full-scale flight (Fig.14). The static pitching-moment derivative m_w and the manoeuvre margin can be adjusted easily to relate to a different centre of gravity position, but the rotary damping derivatives m_q and $m_{\dot{w}}$ can be adjusted with much less certainty. This is the principal disadvantage of testing models in flight with their centres of gravity in an unrepresentative position. In this case the rotary damping measurements are unlikely to have been affected very much. The contributions from the wing and body are relatively insensitive to small movements of the centre of gravity, and the contribution from the tail is nearly proportional to the tail arm. Hence the measurements probably differ by no more than 5 per cent from what they would have been if the model centres of gravity had been at $\bar{\bar{c}}/4$. This is considerably less than the experimental uncertainty.

All the free-flight measurements include contributions from the tail which, in the case of the pitching-moment derivatives and the manoeuvre margin, dominate the contributions from the wing-body combination. It would have been feasible to fly a tailless model and to measure its longitudinal stability, and in retrospect it seems a pity that this was not done. The longitudinal short-period frequencies of the individual models (Fig.12) are virtually indistinguishable from each other, although the centres of gravity were spread over a

range of 0.07 $\bar{\bar{c}}$. The total damping measurements (Fig.13) are more scattered than those of frequency and it is clear that the damping of Model 4, which had the cambered and twisted wing, was consistently lower than that of the models with plane wings at all Mach numbers. It is impossible now to determine how far this is due to a reduction in the damping of the wing-body combination and how far to a reduction in the contribution to the damping from the tail.

A feature of the total damping measurements is the sharp change of damping at high subsonic speeds. There is no reason to doubt this, although the low level is indicated by only two measurements from Model 1; the other measurement from this model, at $M = 1.04$, fits into the pattern established by Models 2, 3 and 4. The curve of reduced undamped frequency (Fig.14) reflects principally the short-period frequency curve, because the frequencies were so high. There is a distinct peak just above sonic speed in both curves.

Apart from some scatter at Mach numbers between 1.0 and 1.05, the curves of z_w, m_w and manoeuvre margin (Figs.15, 16 and 17) are generally well defined by the experimental measurements and at Mach numbers up to 1.2 the results from all four models are consistent. The differences in geometry between Model 1 and the other models do not appear to have had any significant effect, but the evidence is not sufficient to prove the point beyond doubt. At Mach numbers above 1.2 the measurements from the plane wing (Models 1, 2 and 3) and the cambered and twisted wing (Model 4) tend to differ. This is most easily seen in Fig.17.

The rotary damping measurements (Fig.18) rise to a peak near sonic speed, and fall gradually as the Mach number increases. At high subsonic speeds there is a sharp fall to zero damping. A transonic loss of rotary damping is consistent with the behaviour of other swept wings[9], but the steepness of the drop and the sharpness of the peak are unusual.

A characteristic of all the models is that the transonic shift of aerodynamic centre occurred in two distinct stages, one just below $M = 1$ and the other between $M = 1.1$ and $M = 1.25$. At each stage an increase in pitching moment was accompanied by a loss of lift, and the subsonic stage also coincided with the sharp change of rotary damping.

In comparing the free-flight measurements with the wind-tunnel test results (Fig.20) it must be remembered that not only were the test conditions different but the model afterbodies were different also. The difference in

body shape is likely to have affected the downwash at the tail and hence the longitudinal stability derivatives.

The two sets of z_w measurements (Fig.20a) agree reasonably well at Mach numbers below 1.0 and very well at Mach numbers above 1.2. Between these Mach numbers the flight measurements indicate a well-defined peak at about $M = 1.13$ which is not shown by the tunnel measurements. The flight measurements are also very scattered at Mach numbers close to 1.0. This suggests that z_w varies rapdily with Mach number in this region but, since the method of analysis of the flight records fails when the derivatives change rapidly, the magnitudes of the variations may not have been indicated reliably. The m_w measurements from the two kinds of test agree at Mach numbers below 0.9 and above 1.3 (Fig.20b). At the intermediate Mach numbers the two sets of measurements seldom agree exactly although they indicate the same trends. Probably the most significant difference is in the subsonic Mach number at which the first shift of aerodynamic centre occurred. In the tunnel this was about $M = 0.92$, but in free flight it was about $M = 0.98$ and the shift was then more pronounced. The measurements of manoeuvre margin (Fig.20c) reflect the m_w measurements, and the curves through the two sets of data differ at most Mach numbers. However, the differences in H_m do not exceed 0.05 except at $M = 0.94$.

The curves of the static derivatives for the wing-body combination (Fig.23) were obtained from the free-flight measurements by estimating the contributions from the tail in the simplest way possible. Since these curves were to be compared with measurements obtained in the tunnel from models with different afterbodies, more elaborate methods of estimation seemed pointless. In the event the simple estimates have yielded curves which agree reasonably well with the wind-tunnel curves. Moreover, significantly better agreement was not obtained either by using the tail contributions that were measured in the tunnel, or by using the tunnel measurements of $\partial\varepsilon/\partial\alpha$ to estimate the tail contributions. (The curves obtained by these alternative methods have been omitted from Fig.23 for clarity.) Nevertheless, it should be emphasised that the agreement in Fig.23b must be quite sensitive to comparatively small changes in the estimated tail contribution.

The comparison between the free-flight measurements from the swept-wing and the M-wing models (Fig.25) indicates some of the qualitative differences between the characteristics of the two kinds of aircraft. Both configurations

experienced a loss of lift at low supersonic speeds but the loss from the M-wing model, and the associated rearward movement of the aerodynamic centre, was more abrupt than that from the swept-wing and occurred at lower Mach numbers. The M-wing model yielded smaller values of m_w and manoeuvre margin, and larger values of rotary damping, than the swept-wing models. These characteristics together indicate a stronger downwash at the tail behind the M-wing than behind the swept-wing. The large differences in m_w and manoeuvre margin between the two configurations is likely to be due partly to the difference in downwash at the tail and partly to the different contributions from the wings. The M-wing is shorter in length than the swept-wing and, at a given C_L, the pitching moment produced by the loading on it must be correspondingly smaller.

More detailed interpretation of Fig.25 requires caution because the tail arm of the M-wing model, measured from $\bar{\bar{c}}/4$, was longer than that of the swept-wing models by about 0.2 $\bar{\bar{c}}$ (see section 4). It is likely that there were also considerable differences between the aeroelastic properties of the two kinds of wing.

The calculation of the aeroelastic losses of lift and pitching moment from the swept-wing models are important in that they show how large such losses can be, even when the wing is made from solid steel. Clearly, in any test to measure the stability characteristics of a swept-wing model, aeroelastic effects should not be ignored.

7 CONCLUSIONS

7.1 The measurements of m_w, z_w and manoeuvre margin from the four models are self-consistent at Mach numbers up to 1.2. There is some scatter in the measurements at Mach numbers just above 1.0 but, apart from this, the variation of these derivatives with Mach number is well defined. The measurements of rotary damping $(m_q + m_{\dot{w}})$ show a slight fall with increasing Mach number at supersonic speeds; at high subsonic speeds, there is a steep fall to zero damping.

7.2 The principal effects of the particular camber and twist chosen on the longitudinal stability were to reduce the rotary damping at all supersonic speeds and to reduce m_w and the manoeuvre margin at Mach numbers above 1.2. Both effects were slight.

7.3 Measurements obtained in a transonic wind tunnel, from one of the models with its rear body modified, support the free-flight measurements reasonably well. The main difference is that the flight measurements of z_w rise to a distinct maximum at about $M = 1.13$, whereas the tunnel measurements do not.

7.4 Curves of the static derivatives for the wing-body combination were derived from the free-flight measurements by subtracting from them the estimated contributions from the tail. These curves compare well with measurements obtained from the model in the wind tunnel without its tail.

7.5 The free-flight measurements of the pitching-moment derivatives were dominated by the contributions from the tail. Hence the uncertainty with which m_w could be found for the wing-body combination was largely the uncertainty of estimation of the contribution to m_w from the tail. Measurements of m_w for the wing-body combination could have been obtained with less uncertainty from a tailless model, and this would have provided pitch damping measurements as well.

7.6 The losses of lift and pitching moment caused by aeroelastic distortion of the models were found to be significant, even when the wings were made of solid steel. At $M = 1.2$, the reduction in z_w was about 7 per cent and the reduction in m_w was about 15 per cent. In future tests, aeroelastic effects should not be neglected.

7.7 In comparison with an M-wing model with the same gross wing area and a similar body and tail, the swept-winged models had less rotary damping but a larger manoeuvre margin. Through the transonic speed range, the aerodynamic centre of the swept-wing models moved about twice as far as that of the M-wing model, but the movement was less abrupt and continued to a higher Mach number. The lift-curve slope of both kinds of model was virtually the same, although the M wing had a higher aspect ratio.

Appendix A

MODEL GEOMETRY

The wing planform was defined as follows. The trailing edge was straight from root to tip and was swept back 55 degrees. The inboard half of the wing had a constant chord, and the spanwise distribution of chord over the outboard half of the wing was defined by the equation

$$c = 2c_o \left\{ \left[2\left(1 - \frac{y}{s}\right) \right]^{\frac{1}{2}} - \left(1 - \frac{y}{s}\right) \right\}$$

where $0.5 \leq \frac{y}{s} \leq 1.0$.

Chords of the model wings are given in the following table.

Table A1

Ordinates of outboard half of wing planform

y inches	$\frac{y}{s}$	$\frac{c}{2c_o}$	c inches
9.739	0.50	0.50	12.500
10.0	0.5134	0.4999	12.498
10.5	0.5390	0.4992	12.480
11.0	0.5647	0.4977	12.443
11.5	0.5904	0.4955	12.388
12.0	0.6161	0.4924	12.310
12.5	0.6417	0.4882	12.205
13.0	0.6674	0.4830	12.075
13.5	0.6931	0.4766	11.915
14.0	0.7188	0.4687	11.718
14.5	0.7444	0.4594	11.485
15.0	0.7701	0.4482	11.205
15.5	0.7958	0.4349	10.873
16.0	0.8214	0.4191	10.478
16.5	0.8471	0.4001	10.003
17.0	0.8728	0.3772	9.430
17.5	0.8985	0.3491	8.728
17.75	0.9113	0.3326	8.315
18.0	0.9241	0.3137	7.843
18.25	0.9370	0.2920	7.300
18.5	0.9498	0.2667	6.668
18.75	0.9626	0.2361	5.903
19.0	0.9755	0.1969	4.923
19.125	0.9818	0.1724	4.310
19.25	0.9883	0.1413	3.533
19.375	0.9947	0.0981	2.453
19.479	1.0	0	0

The body profile of the basic configuration (Model 1) consisted of an ogival nose, a cylindrical centre portion, and an afterbody which had the same profile as the nose but was cut off where its diameter was one inch. The ogive had the shape, given by slender-body theory, with the least wave drag for a given length and base area. (The von Karman ogive.) Its profile is given by

$$r = \left(\frac{S(x)}{\pi}\right)^{\frac{1}{2}}$$

where $$S(x) = \frac{2B}{\pi}\left\{ \sin^{-1}\left(\frac{x}{\ell}\right)^{\frac{1}{2}} + \left(2\frac{x}{\ell} - 1\right)\left[\frac{x}{\ell}\left(1 - \frac{x}{\ell}\right)\right]^{\frac{1}{2}}\right\}$$

and

$$0 \leq \frac{x}{\ell} \leq 1 \quad .$$

Ordinates of the body of Model 1 are given in the following table:

Table A2 Ordinates of the body of Model 1

Inches aft of nose tip	Body radius (inches)	Inches forward of after-body base
0	0	
1	0.266	
2	0.446	
2.340	0.500	0
3	0.600	0.660
4	0.740	1.660
5	0.870	2.660
6	0.991	3.660
7	1.105	4.660
8	1.214	5.660
9	1.317	6.660
10	1.416	7.660
11	1.510	8.660
12	1.600	9.660
13	1.686	10.660
14	1.768	11.660
15	1.846	12.660
16	1.921	13.660
17	1.993	14.660
18	2.060	15.660
19	2.125	16.660
20	2.186	17.660
21	2.242	18.660
22	2.295	19.660
23	2.344	20.660
24	2.388	21.660
25	2.427	22.660
26	2.460	23.660
27	2.486	24.660
28	2.500	25.660

Models 3, 4 and 5 had bodies of revolution designed by means of the supersonic Area Rule to have the same length, volume and base area as the body of the basic model aircraft (Model 1). The ordinates of these bodies are given in the following table:

Table A3

Ordinates of the bodies of Models 2, 3 and 4

Inches aft of nose	Body radius (inches)	Inches aft of nose	Body radius (inches)
0	0	41	2.349
1	0.288	42	2.332
2	0.486	43	2.323
3	0.659	44	2.319
4	0.816	45	2.319
5	0.960	46	2.321
6	1.093	47	2.323
7	1.216	48	2.325
8	1.331	49	2.326
9	1.439	50	2.326
10	1.540	51	2.324
11	1.635	52	2.320
12	1.725	53	2.312
13	1.810	54	2.301
14	1.890	55	2.286
15	1.966	56	2.266
16	2.038	57	2.242
17	2.107	58	2.213
18	2.172	59	2.179
19	2.234	60	2.141
20	2.292	61	2.098
21	2.347	62	2.051
22	2.399	63	1.999
23	2.448	64	1.943
24	2.496	65	1.883
25	2.538	66	1.819
26	2.579	67	1.751
27	2.616	68	1.679
28	2.650	69	1.604
29	2.679	70	1.525
30	2.703	71	1.443
31	2.719	72	1.356
32	2.724	73	1.264
33	2.710	74	1.165
34	2.678	75	1.058
35	2.631	76	0.940
36	2.573	77	0.815
37	2.512	78	0.690
38	2.457	79	0.573
39	2.411	80	0.500
40	2.375		

The movements of the tailplanes of Models 2, 3 and 4 were limited by fixed stops. The following table gives the tailplane angles, relative to the body axis, when the actuators were against the stops.

Table A4

Tailplane angles of Models 2, 3 and 4

Model No.	2	3	4
Tailplane angles	+0° 12' -5° 48'	+0° 50' -5° 17'	-0° 5' -6° 14'

Appendix B

AEROELASTIC CORRECTIONS

The losses of lift and pitching moment caused by aeroelastic distortion of the wing were calculated by an iterative method adapted from Broadbent's method[13] of finding the loss of rolling moment. It was assumed that the change of loading on the wing was associated only with the change in the distribution of angle of attack across the span, and that chordwise and spanwise bending of the wing could be ignored.

The appropriate stiffness characteristics of a solid steel wing and a laminated aluminium alloy wing were found experimentally. In each case a normal force and a pitching moment were applied separately on three chords in turn, and the changes of angle of attack of all three chords were measured every time the wing was loaded. The normal force was applied on each chord at the point where it caused no local change of angle of attack (Fig.26). The measurements are plotted in Fig.27. Although the two wings were constructed differently there was a marked similarity between the shapes of the curves obtained from them.

For the purpose of computing the aeroelastic effects in flight each wing was divided into seven chordwise strips of equal width, and the aerodynamic loading on each strip was assumed to be concentrated on its centre line (Fig.26). Curves relating the change of angle of attack of each of the strip centre lines to the spanwise positions of both kinds of unit load were obtained by cross-plotting from Fig.27. The ordinates of these curves at the spanwise positions of the seven strip centre lines were the values of θ_{RS} used in the subsequent calculations.

Since there were no experimental measurements of the load distribution on the wing, the aeroelastic losses of lift and pitching moment were computed only for the design conditions of a uniform initial distribution of C_L across the span and the chordwise load distribution of Fig.4. There is evidence[2,5] to show that these conditions were largely fulfilled at Mach numbers near 1.2. The initial theoretical loading on each strip was expressed in the form of a lift force and the moment of that force about the point on the strip centre line where the force would cause no change of angle of attack. To simplify the numerical working it was assumed that $\frac{1}{2}\rho V^2 = 1000$ lb/ft^2 and $C_L = 1$.

The change of angle of attack of each strip, caused by the initial loading on the whole wing, is given by

$$\Delta\alpha_R = \sum_{s=1}^{s=7} L_S \, (\theta_{RS})_L + \sum_{s=1}^{s=7} M_S \, (\theta_{RS})_M \quad . \tag{13}$$

The resultant change of lift is

$$\Delta L_R = \tfrac{1}{2}\rho V^2 S_R \frac{\partial C_L}{\partial \alpha} \Delta\alpha_R \tag{14}$$

and the change of moment, about the point where ΔL_R causes no local change of angle of attack, is

$$\Delta M_R = \Delta L_R \, (x_L - x_F)_R \quad . \tag{15}$$

These quantities were calculated for each strip, using a value of 3.5 for $\partial C_L/\partial\alpha$. To preserve order in the working it was convenient to arrange the numbers in matrices. The process was repeated to find the additional changes of angle of attack caused by the loads ΔL and ΔM, and so on until the numbers became negligible. The aeroelastic losses of lift and pitching moment were then given by the algebraic sums of all the incremental lift forces such as ΔL_R and of their moments about $\bar{\bar{c}}/4$. In the following table the losses are compared to the initial loading on the undistorted gross wing and expressed in terms of the derivatives m_w and z_w.

Table B1

Estimated corrections at M = 1.2 for the effects of aeroelastic distortion of the wing only

		Laminated Al-alloy wing (Model 1)	Solid steel wing (Models 2, 3 and 4)
Aeroelastic losses from gross wing	$\frac{\Delta L}{L}\left(\propto \frac{\Delta z_w}{z_w}\right)$	-0.196	-0.067
	$\frac{\Delta M}{M}\left(= \frac{\Delta m_w}{m_w}\right)$	+1.3	+0.46
Derivatives for undistorted gross wing	Assumed value of z_w	-1.75	-1.75
	Corresponding theoretical m_w (referred to $\bar{\bar{c}}/4$)	-0.208	-0.208
Corrections to be added to measurements	Δz_w	-0.34	-0.12
	Δm_w	-0.28	-0.10

The reduction of tailplane angle of attack, caused by body bending, was calculated theoretically by treating the body aft of the wing root as a cantilever. The extra stiffness afforded by the fin was allowed for arbitrarily by assuming that the lift on the tail acted at the apex of the tailplane. The reduction of tailplane angle of attack is given by

$$\Delta\alpha_T = -\frac{L_T}{E}\int_A^B \frac{x}{I}\,dx \quad , \tag{16}$$

where the limits A and B refer to the tailplane apex and the wing root trailing edge respectively. The body was treated as a continuous shell 0.25 inch thick. The corresponding loss of tailplane lift is given by

$$\Delta L_T = \left(\frac{\partial C_L}{\partial\alpha}\right)_T \Delta\alpha_T \quad . \tag{17}$$

These quantities were calculated for an arbitrary initial angle of attack. They were then repeated to find the change of angle associated with ΔL_T, then the resultant change in lift, and so on until the numbers became negligible. This showed a reduction of approximately 4 per cent in the tailplane angle of attack due to body bending.

The stiffness of the tailplane was not measured, but was estimated by reference to measurements made on other models of the same kind (e.g. Model 3 of Ref.14). These indicated that the tailplane shed about 3 per cent of its lift. Hence the total loss of lift from the tailplane, caused by aeroelastic distortion of the body and tail, was about 7 per cent. The resultant reductions in m_w and z_w on the complete model were calculated from the estimates of the contributions from the tail to these derivatives, given by equations (7) and (8). They are shown graphically in Fig.22.

The total effect of aeroelastic distortion of the wing, body and tail is summarised in the following table and shown graphically in Figs.15, 16 and 17. These estimates relate only to a Mach number of 1.2, since it was not practicable to calculate the effect of wing distortion at any other Mach number. They refer only to the models with steel wings, because the experimental results were obtained entirely from these models at Mach numbers above 1.04.

Table B2

Summary of aeroelastic corrections at M = 1.2

	Δm_w	Δz_w
Steel wing only	-0.10	-0.12
Body and tail	-0.058	-0.022
Complete model	-0.158	-0.142

The effect of aeroelasticity on the manoeuvre margin was found approximately by calculating the static margin, given by equation (12), from the corrected values of m_w and z_w.

At Mach numbers below 1.2 the aerodynamic centre moved forward and the aeroelastic losses would have been slightly smaller; at higher Mach numbers the aerodynamic centre moved aft, with correspondingly larger losses. The range of variation of the losses was probably less than ±10 per cent, and the corrections given in Table B2 remain a good approximation at all supersonic Mach numbers. At Mach numbers below 0.97 the free-flight measurements were all from Model 1, which had the laminated aluminium-alloy wing. An approximation to the appropriate corrections may be obtained by reducing the corrections calculated for this wing at M = 1.2 (Table B1) by 10 per cent to allow for the forward position of the aerodynamic centre at subsonic speeds.

The aeroelastic corrections were calculated for static loading conditions, whereas the flight measurements were made while the models were oscillating at frequencies between 4.5 and 9 Hz (Fig.12). However the measured fundamental bending frequencies of the laminated and the solid wings were respectively 26 and 30.3 Hz, and those of the body and tailplane were much higher. Thus the oscillation frequencies were always so far below the resonance frequencies that the distortion of the models under the oscillatory loading was not significantly different from the distortion under the same loading applied statically. The static corrections can therefore be applied to the dynamic measurements.

Appendix C

MODEL WEIGHT AND INERTIA CHARACTERISTICS

Model number	1	2	3	4
Weight (lb)	88.1	136.0	133.7	132.2
cg position, as a fraction of $\bar{\bar{c}}$	0.139	0.075	0.147	0.136
Moments of inertia				
Roll, A (slug ft^2)	0.488	1.295	1.217	1.334
Pitch, B (slug ft^2)	5.836	6.808	6.461	6.487
Yaw, C (slug ft^2)	6.004	8.010	7.652	7.624
Inertia coefficients				
i_A (= A/m s^2)	0.0677	0.116	0.111	0.123
i_B (= B/m $\bar{\bar{c}}^2$)	2.199	1.662	1.604	1.629
i_C (= C/m s^2)	0.833	0.720	0.700	0.705

SYMBOLS

A	moment of inertia in roll
B	moment of inertia in pitch; base area of ogive
c	local wing chord
c_o	wing root chord
$\bar{\bar{c}}$	aerodynamic mean chord $= \int c^2\, dy \Big/ \int c\, dy$
C	moment of inertia in yaw
C_D	drag coefficient $= D/\frac{1}{2}\rho V^2 S$
C_L	lift coefficient $= L/\frac{1}{2}\rho V^2 S$
C_m	pitching moment coefficient $= M/\frac{1}{2}\rho V^2 S \bar{\bar{c}}$
C_p	pressure coefficient $= (p - p_s)/\frac{1}{2}\rho V^2$
D_1	distance from centre of gravity to focal point
E	Young's modulus
H_m	manoeuvre margin $= \frac{m_w}{z_w} - \frac{m_q}{\mu_1}$
H_n	static margin $= \frac{m_w}{z_w}$
i_A	$= A/m\, s^2$
i_B	$= B/m\, \bar{\bar{c}}^2$
i_C	$= C/m\, s^2$
I	second moment of body cross-section area about a diameter parallel to the plane of the wing
ℓ	ogive length
ℓ_T	tail arm (between $\bar{\bar{c}}/4$ and aerodynamic centre of tailplane)
L	lift force
L_S	lift on strip S
L_T	lift force on the tail
m	aircraft mass
m_q	$= M_q/\rho V S \bar{\bar{c}}^2 = \frac{1}{2}\, \partial C_m/\partial \left(\frac{q\bar{\bar{c}}}{V}\right)$
m_w	$= M_w/\rho V S \bar{\bar{c}} = \frac{1}{2}\, \partial C_m/\partial \alpha$

SYMBOLS (Contd.)

$m_{\dot{w}}$	$= M_{\dot{w}}/\rho\ S\ \bar{c}^2 = \frac{1}{2}\ \partial C_m/\partial\left(\frac{\dot{w}\ \bar{c}}{V^2}\right)$
M	Mach number; pitching moment
MHz	megahertz
M_q	$= \partial M/\partial q$
M_S	moment on strip S
M_w	$= \partial M/\partial w$
$M_{\dot{w}}$	$= \partial M/\partial \dot{w}$
p	local static pressure; rate of roll
p_s	static pressure of undisturbed air
q	rate of pitch
s	semi-span of gross wing
S	gross wing area
S_R	area of strip R
S_T	tailplane area
S(x)	body cross-section area at station x
$\hat{t}$	$= m/\rho\ S\ V$
V	flight velocity
w	downward velocity
x, y, z	Cartesian coordinates with origin at $\bar{c}/4$; forward, to starboard and downward respectively
x_F	x-coordinate of the point on a specified chord where a normal force causes no local change of angle of attack
x_L	x-coordinate of the load centre of a specified strip
z_w	$= Z_w/\rho\ S\ V = -\frac{1}{2}\left(\frac{\partial C_L}{\partial \alpha} + C_D\right)$
Z	normal force
Z_w	$= \partial Z/\partial w$
α	angle of attack
α_R	angle of attack of centre line of strip R
α_T	angle of attack of the tailplane
ε	downwash angle

SYMBOLS (Contd.)

θ_{RS} change of angle of attack of chord R due to unit load on chord S

λ_1 exponential index of longitudinal damping

μ_1 density ratio in longitudinal equations = $m/\rho S \bar{c}$

ν_1 frequency of the longitudinal short-period oscillation

ρ density of undisturbed air

ω_1 $= 2\pi \nu_1$

ω_{n1} longitudinal undamped natural frequency = $(\omega_1^2 + \lambda_1^2)^{\frac{1}{2}}$

REFERENCES

No.	Author	Title, etc.
1	J.A. Bagley	An aerodynamic outline of a transonic transport aeroplane. R.A.E. Technical Note Aero 2472 (A.R.C. 19205) (1956)
2	G.K. Hunt	A free-flight investigation of wing-body junction design for a transonic swept-wing aircraft. A.R.C. C.P. 759 (1963)
3	W.T. Lord	On the design of wing-body combinations of low zero-lift drag rise at transonic speeds. A.R.C. R & M 3279 (1959)
4	G.M. Roper	Formulae for calculating the camber surfaces of thin sweptback wings of arbitrary planform with subsonic leading edges and specified load distribution. A.R.C. R & M 3217 (1959)
5	A.B. Haines J.C.M. Jones	Transonic tunnel tests on a 6% thick, warped 55° sweptback-wing model. A.R.C. R & M 3385 (1960)
6	J.A. Hamilton P.A. Hufton	Free-flight techniques for high-speed aerodynamic research. Journal, R.Ae.S., 60, 151-185 (1956)
7	A. Stanbrook	The lift-curve slope and aerodynamic centre position of wings at subsonic and supersonic speeds. R.A.E. Technical Note Aero 2328 (A.R.C. 17615) (1954)
8	J.H.B. Smith J.A. Beasley A. Stevens	Calculations of the lift slope and aerodynamic centre of cropped delta wings at supersonic speeds. A.R.C. C.P. 562 (1960)
9	H.H.B.M. Thomas B.F.R. Spencer	The calculations of the derivatives involved in the damping of the longitudinal short-period oscillations of an aircraft and correlation with experiment. R.A.E. Report Aero 2561 (A.R.C. 18498) (1955)

REFERENCES (Contd.)

No.	Author	Title, etc.
10	J.B.W. Edwards	Free-flight measurements of the drag and longitudinal stability of a transonic M-wing aircraft. A.R.C. C.P. 773 (1963)
11	G.K. Hunt	Free-flight measurements of the incremental drag due to engine nacelles on a transonic swept-wing aircraft. A.R.C. C.P. 960 (1966)
12	J. Picken	The uncertainty of processed data from free-flight experiments. R.A.E. Technical Note Aero 2604 (1959)
13	E.G. Broadbent	The rolling power of an elastic swept wing. A.R.C. R & M 2857 (1950)
14	K.J. Turner G.K. Hunt	Free-flight measurements of the transonic roll-damping characteristics of three related wings of aspect ratio 2.83. A.R.C. R & M 3274 (1960)

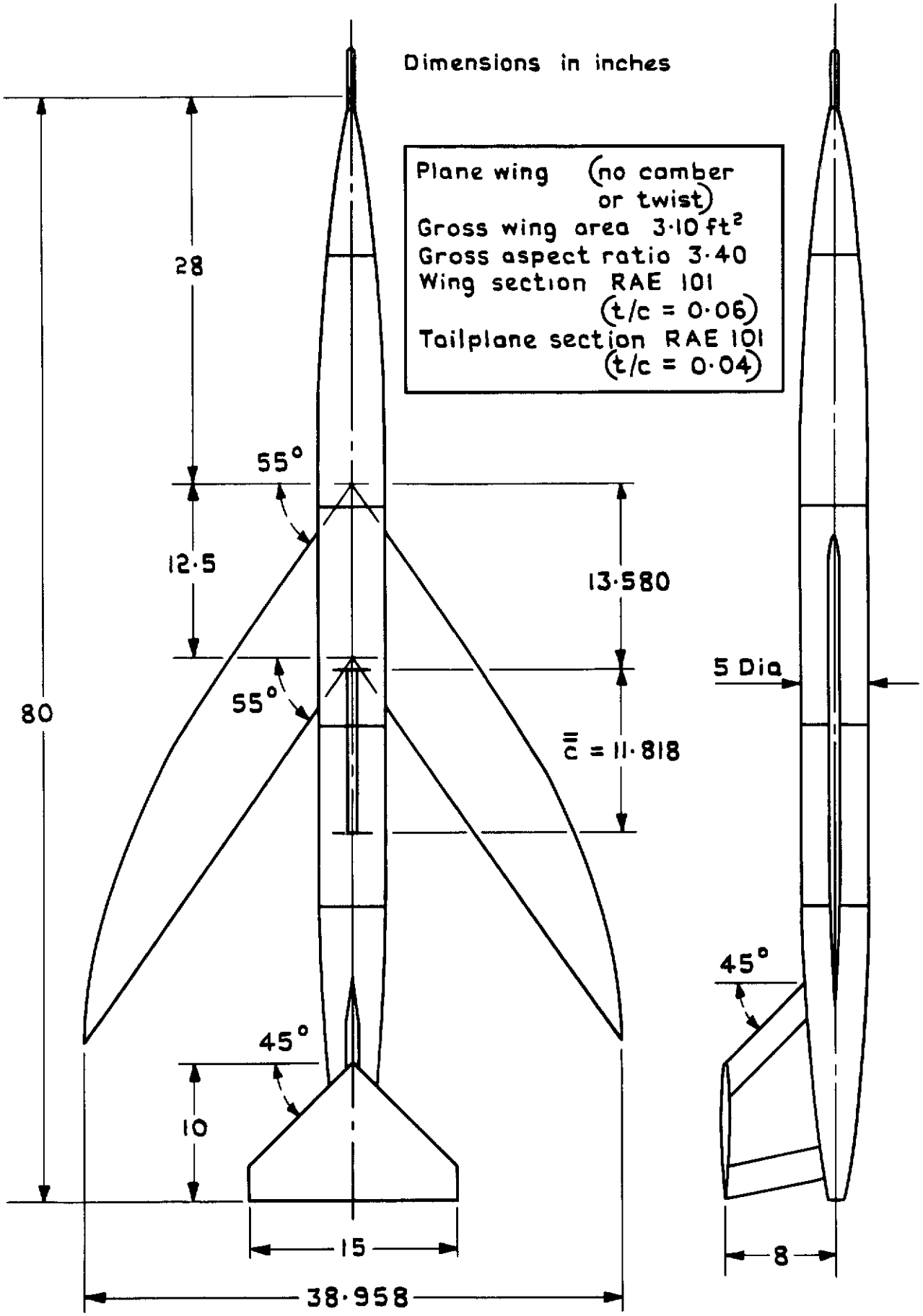

a Model 1

Fig. 1 General arrangement of the models

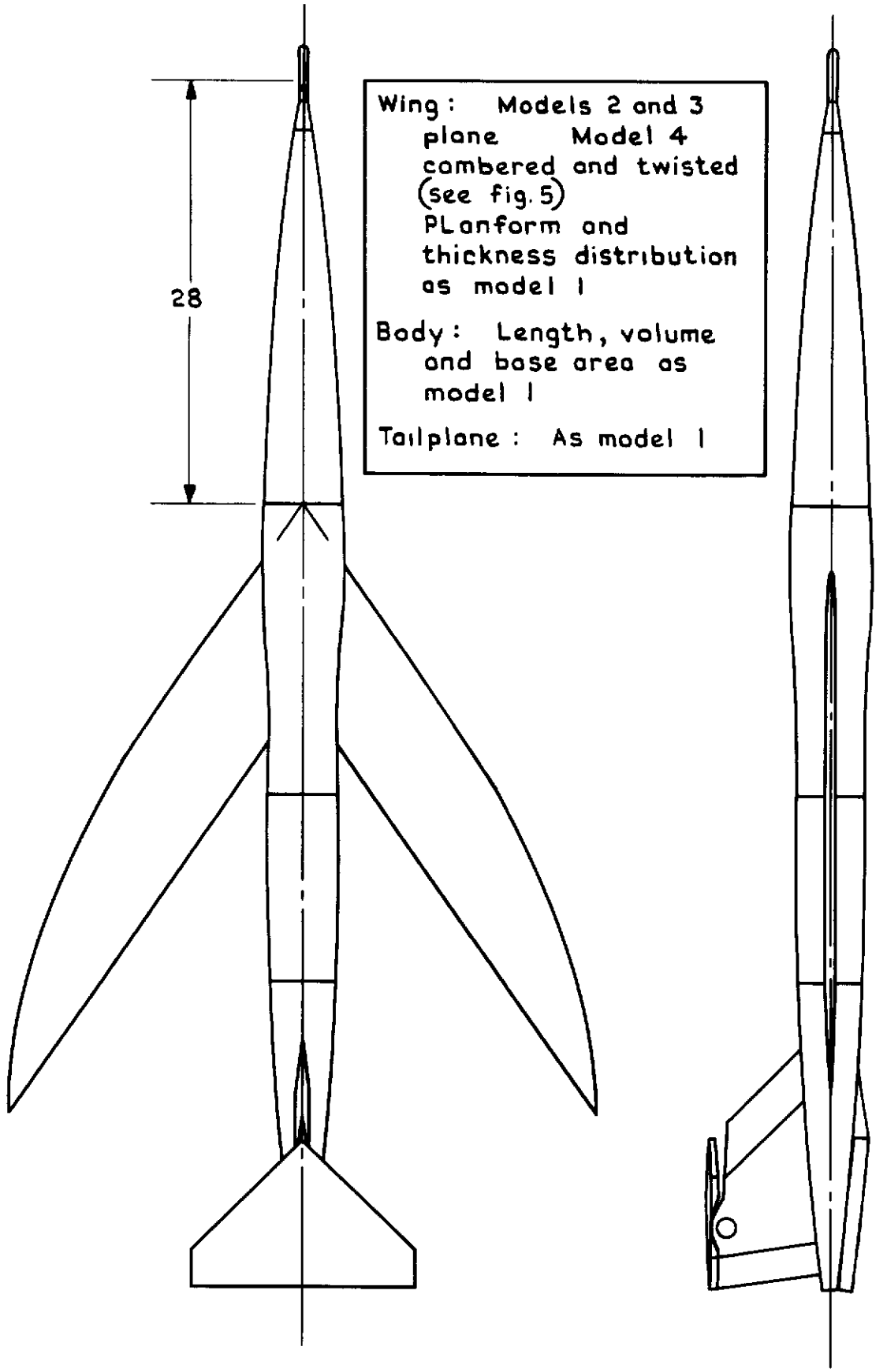

b Models 2, 3 and 4

Fig. 1 contd

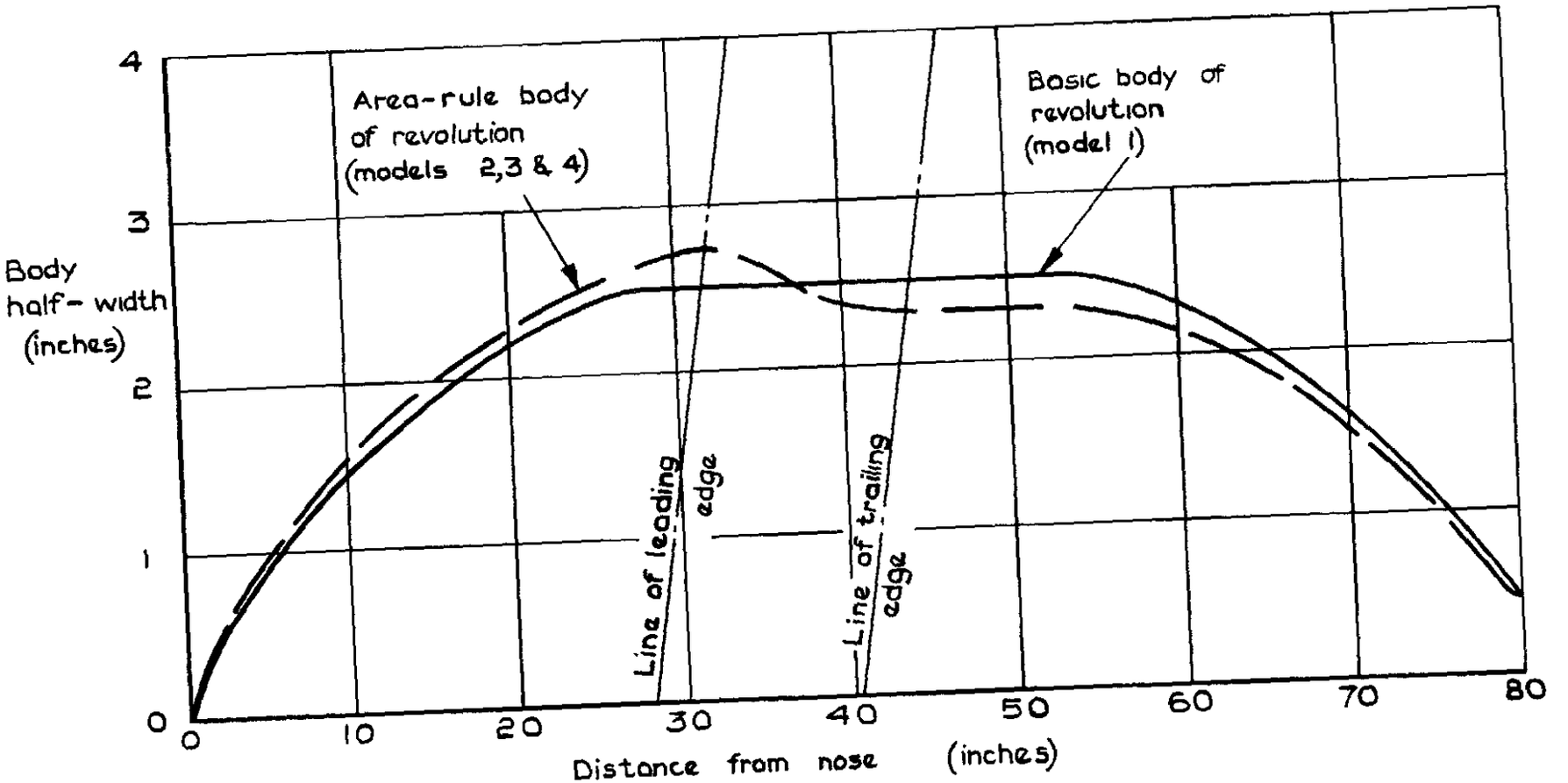

Fig. 2 Body profiles

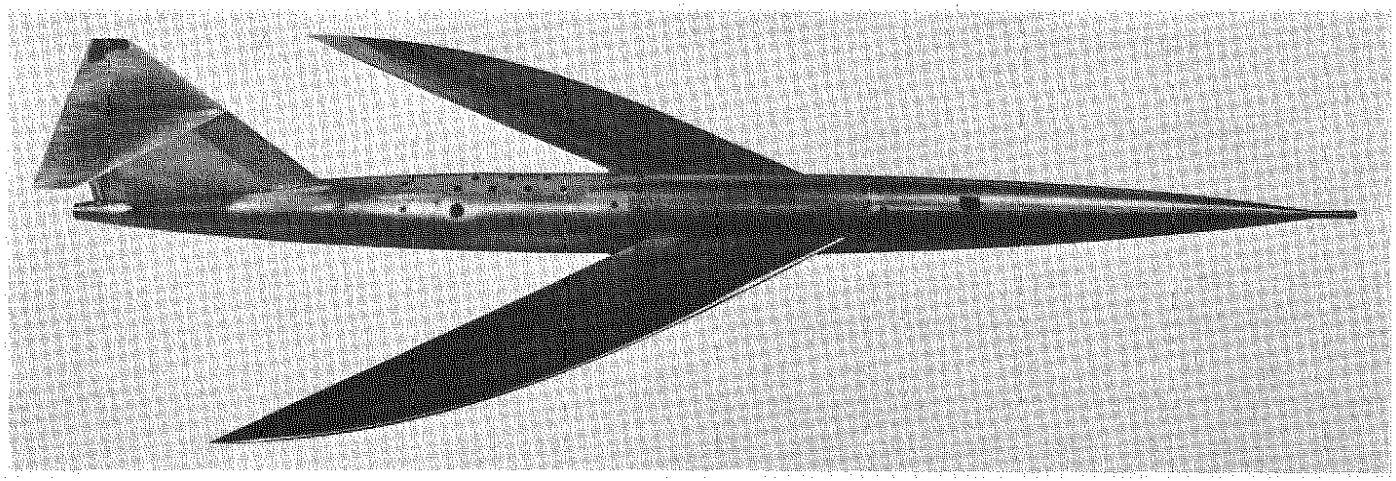

Model 1

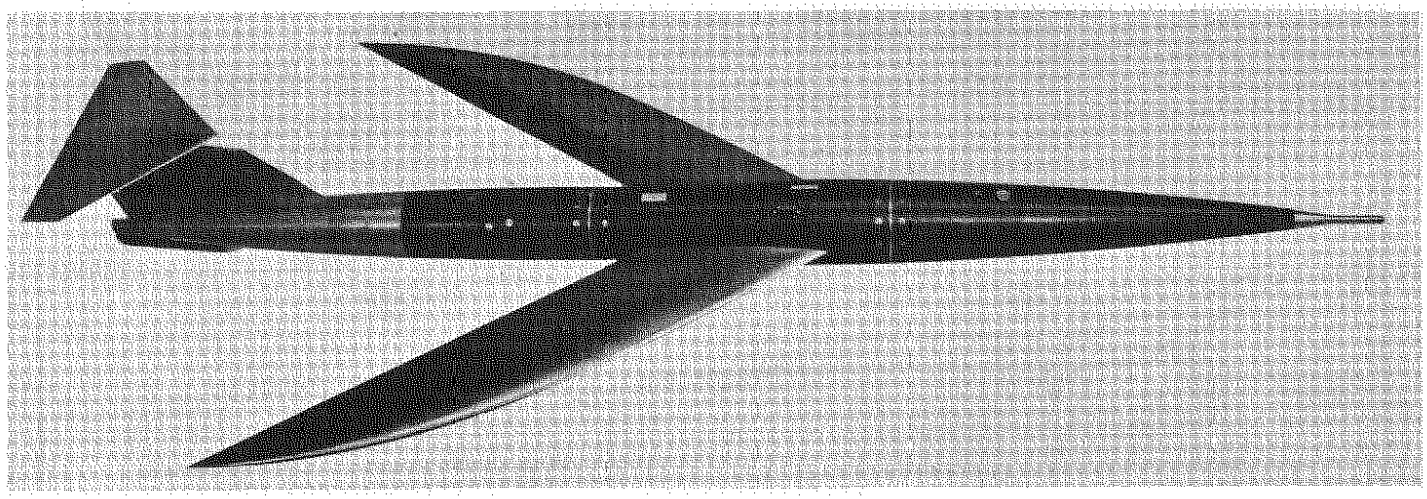

Model 3
(model 2
similar)

Model 4

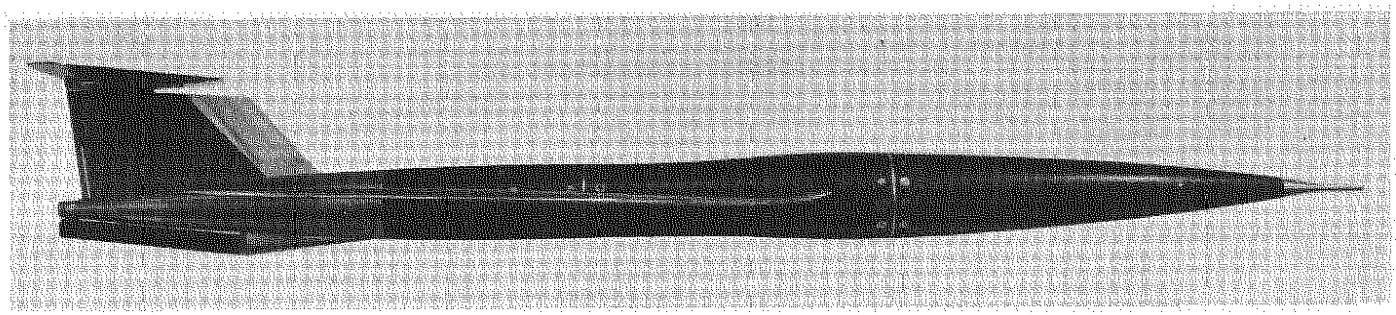

Fig.3. Photographs of the models

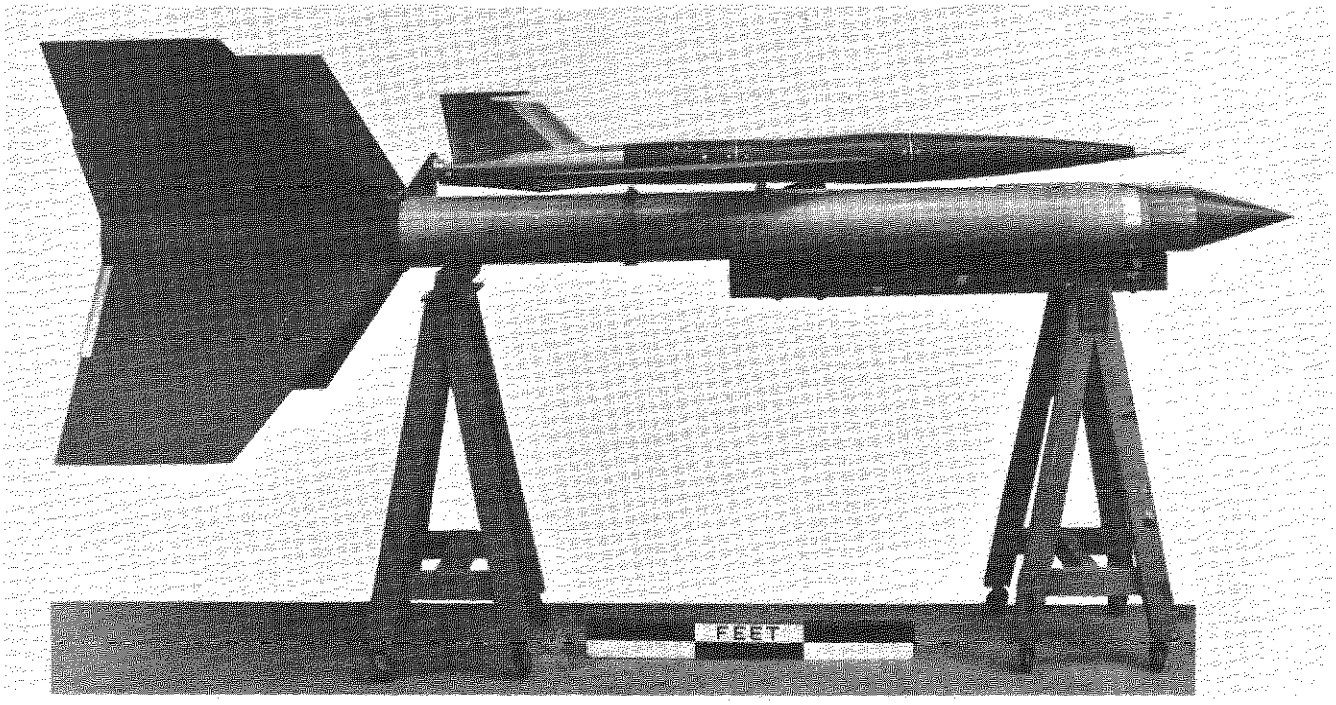

Model 2 with its booster rocket attached

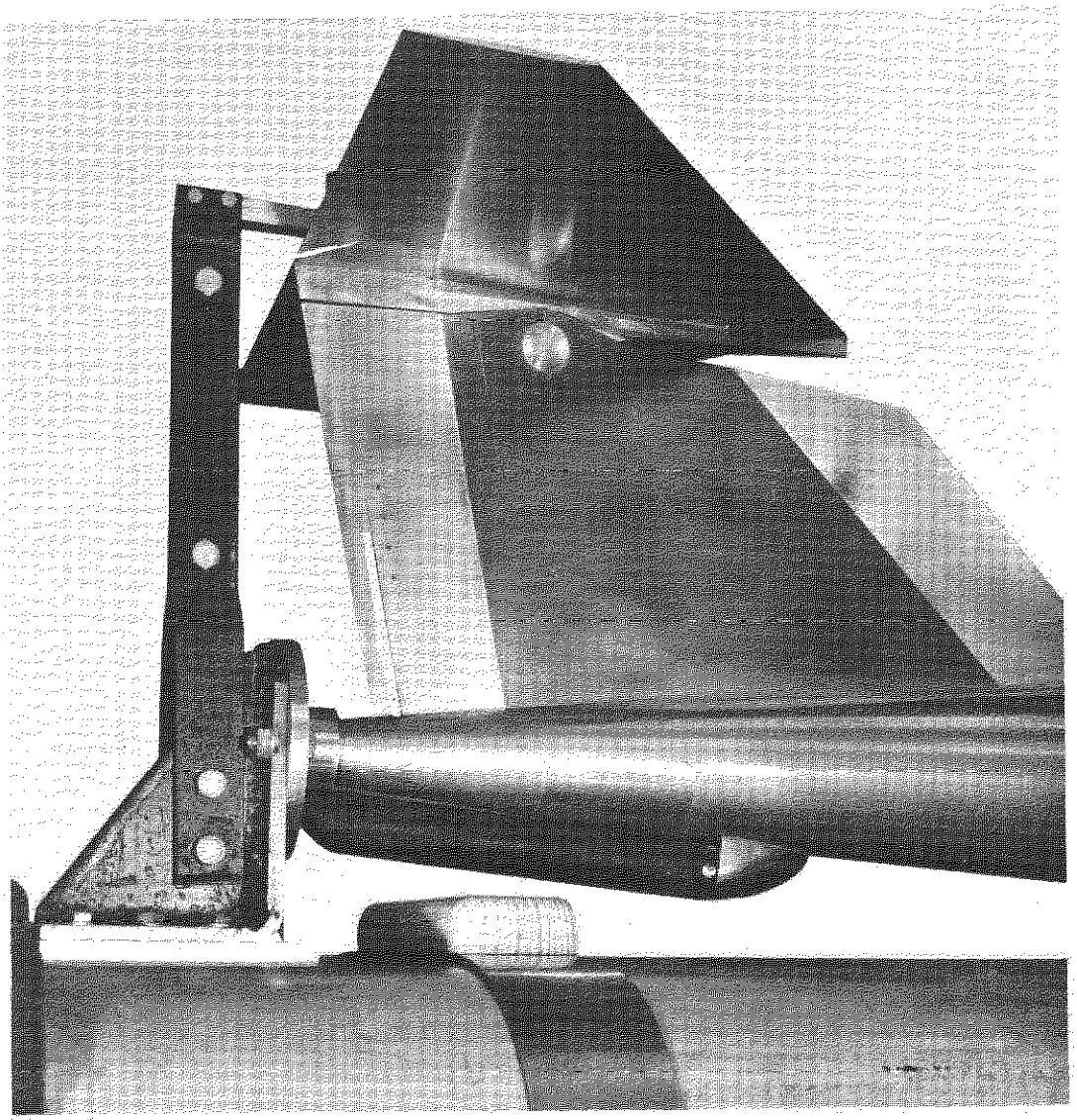

The tail of model 3, showing the attachment to the booster rocket

Fig.3 (cont'd.)

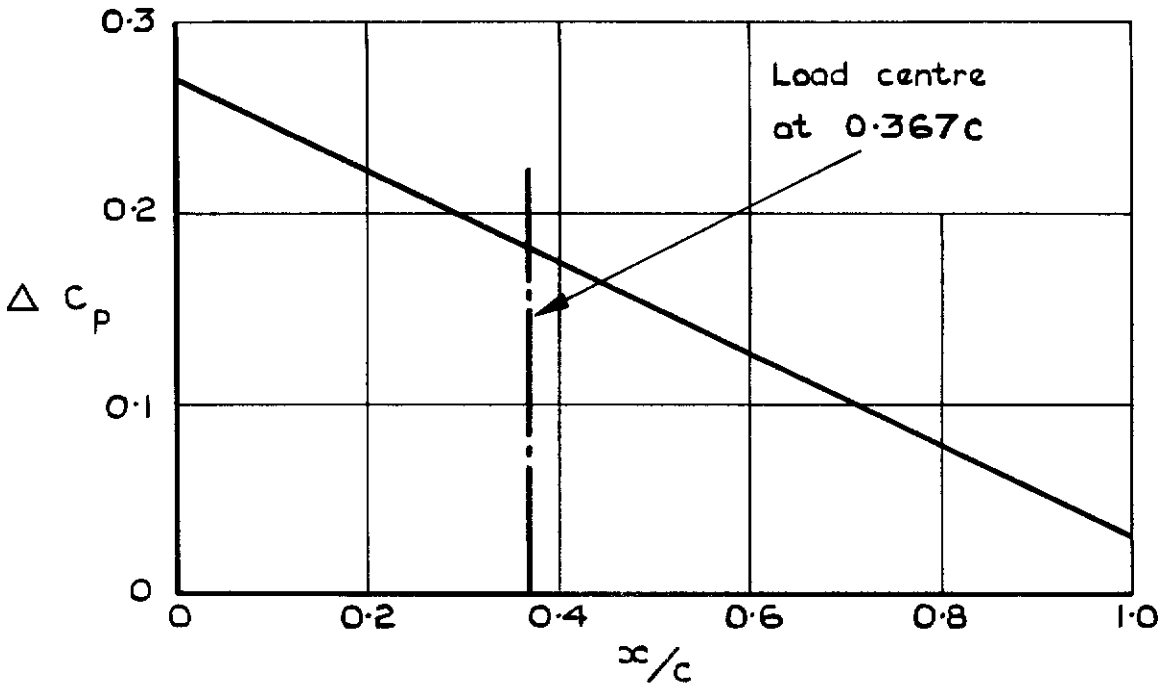

Fig. 4 Cambered and twisted wing (model 4) theoretical chordwise load distribution

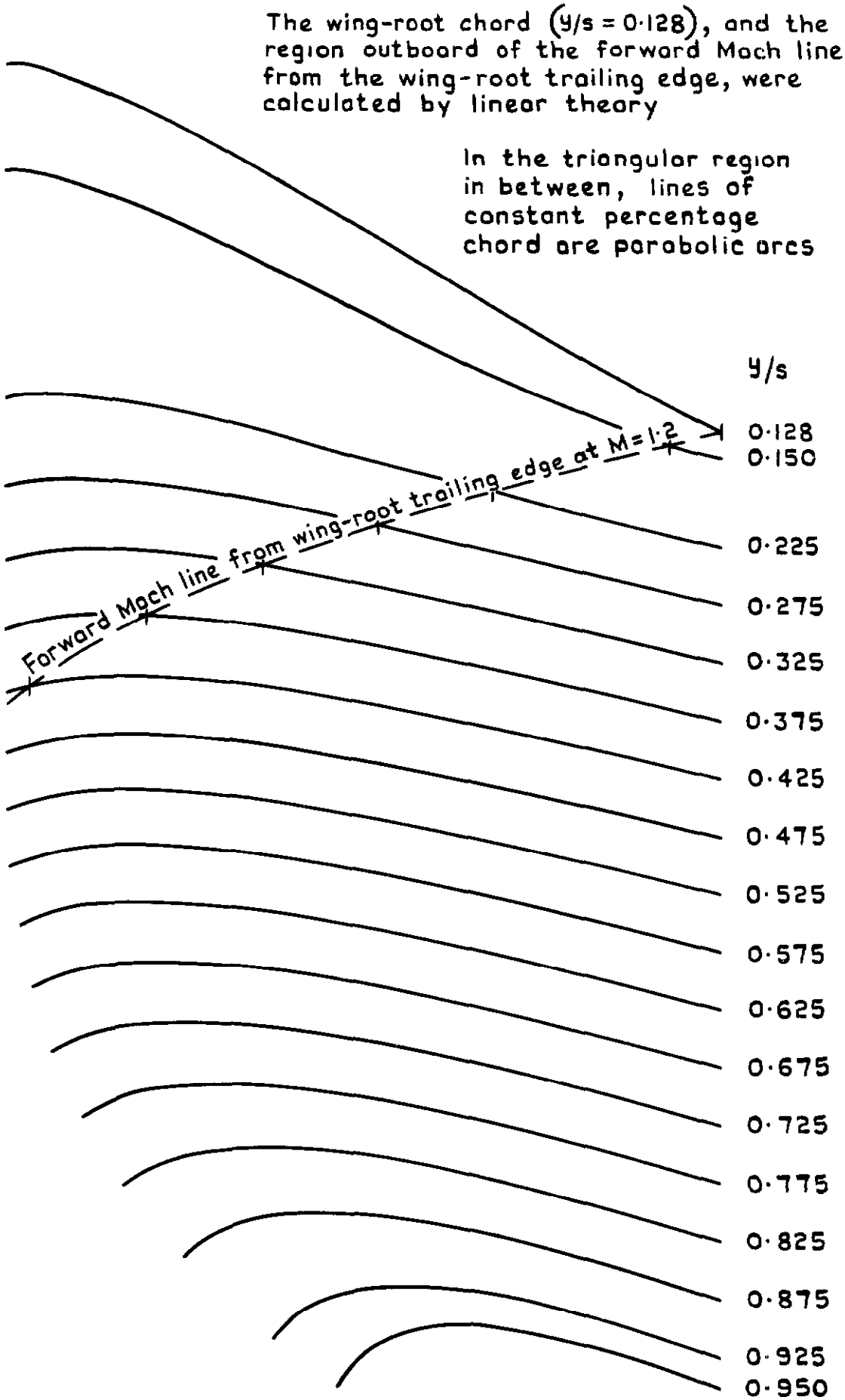

Fig. 5 Cambered and twisted wing (model 4) Median lines of sections, drawn at angle of attack for $C_L = 0{\cdot}15$ (Vertical scale = 5 x horizontal scale)

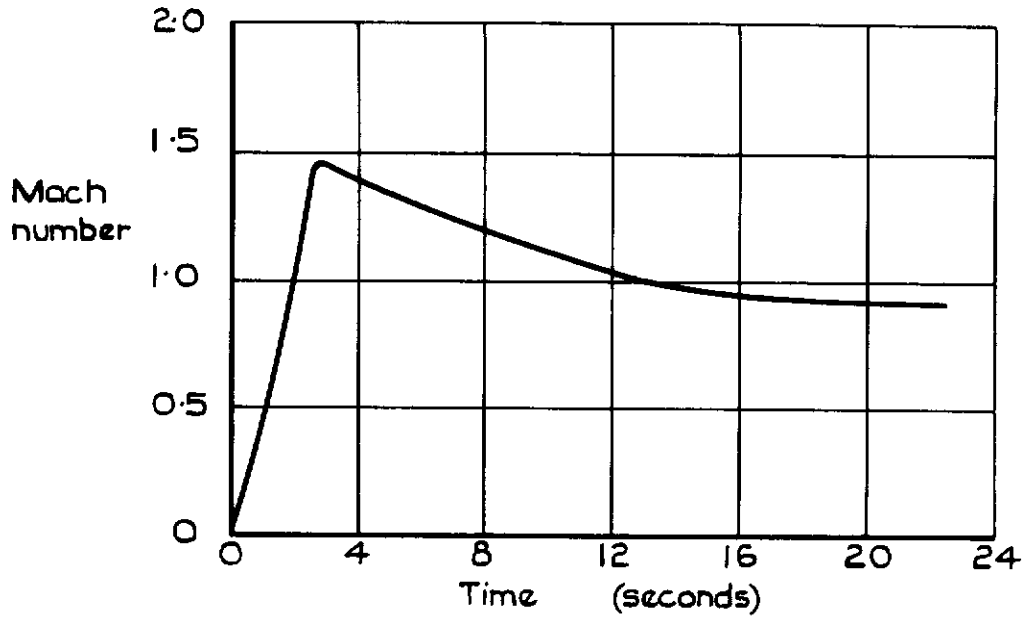

Fig. 6 Typical variation of flight Mach number with time (model 3)

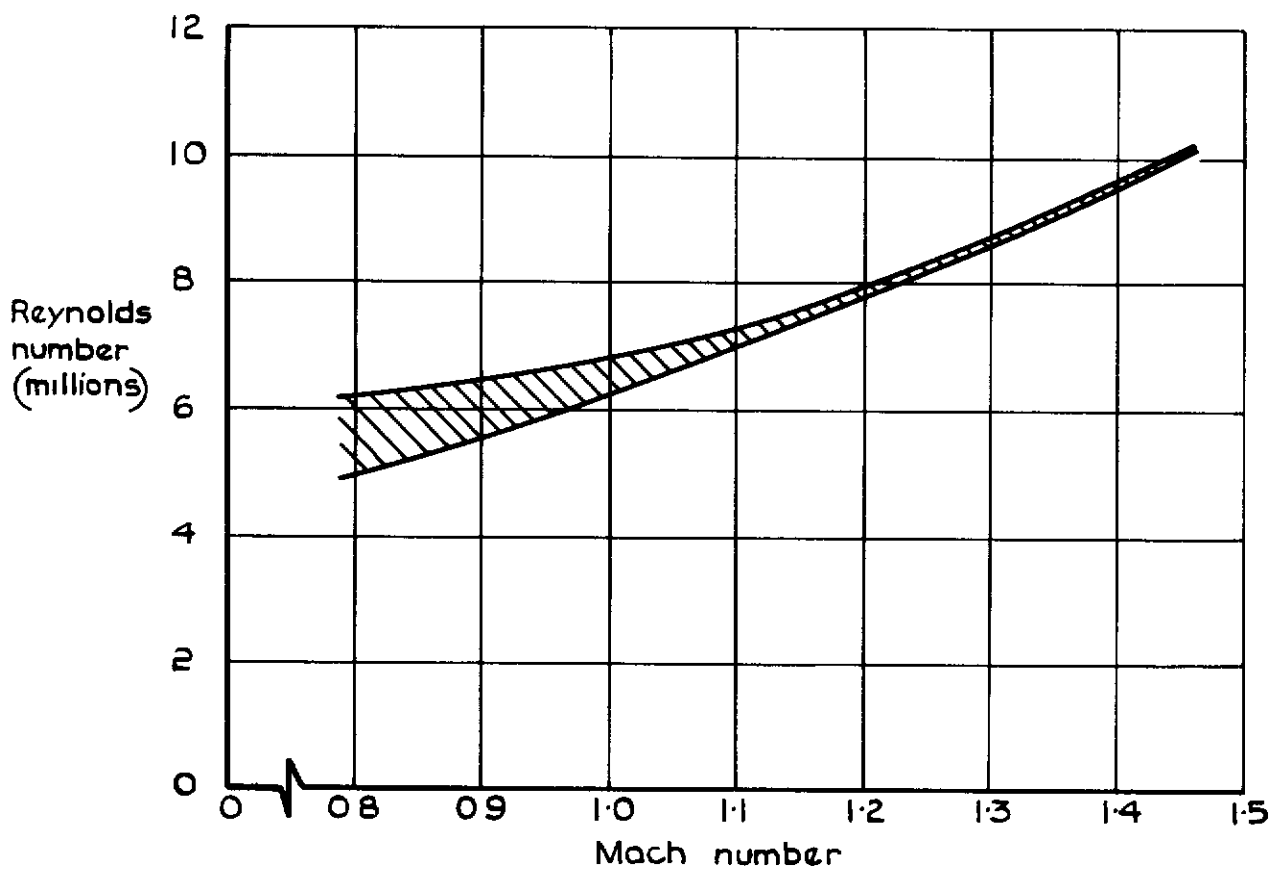

Fig. 7 Flight Reynolds number (based on $\bar{\bar{c}}$)

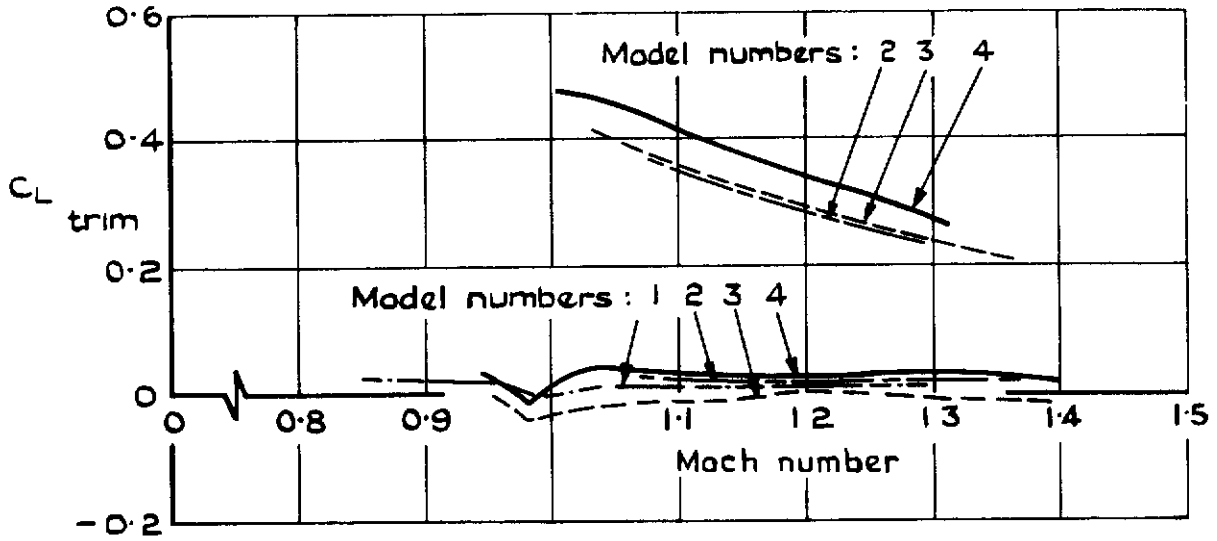

Fig.8 Trimmed lift coefficient

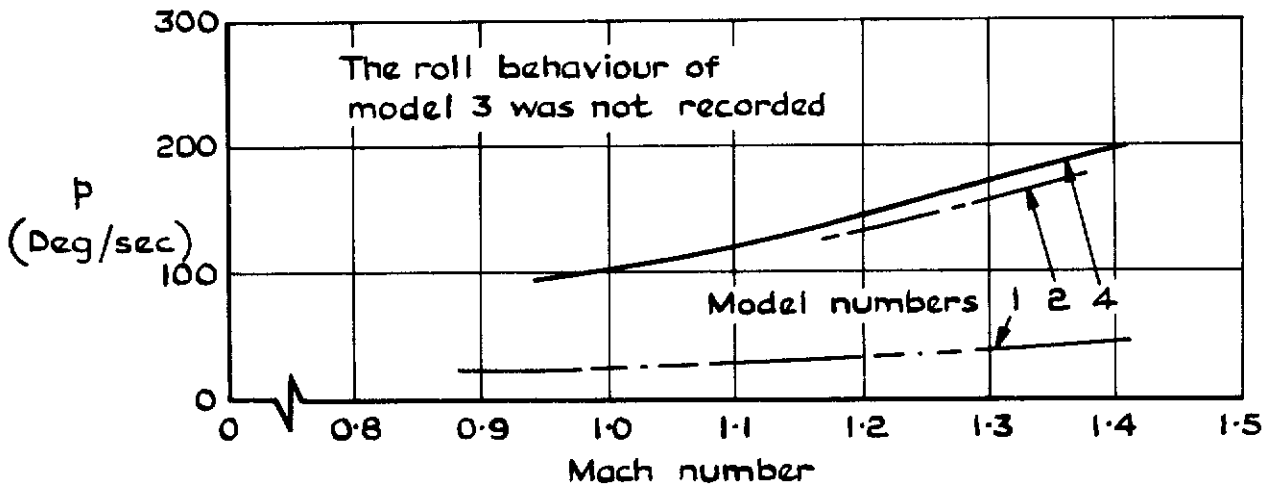

Fig.9 Mean rate of roll

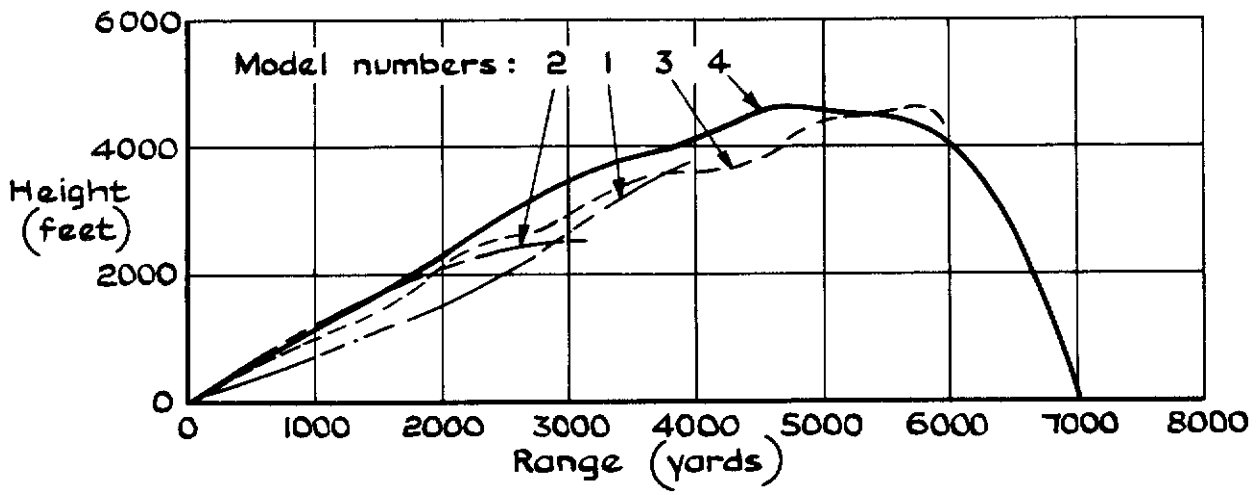

Fig.10 Flight paths

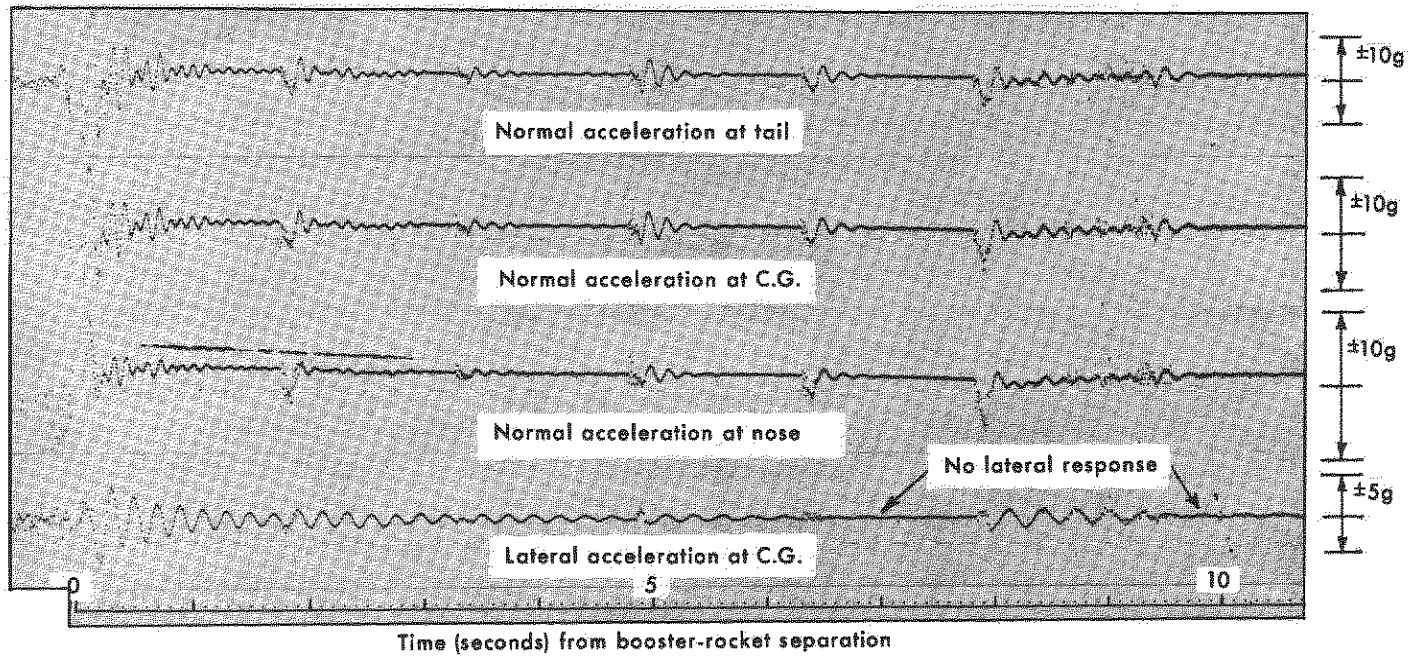

a. Model 1

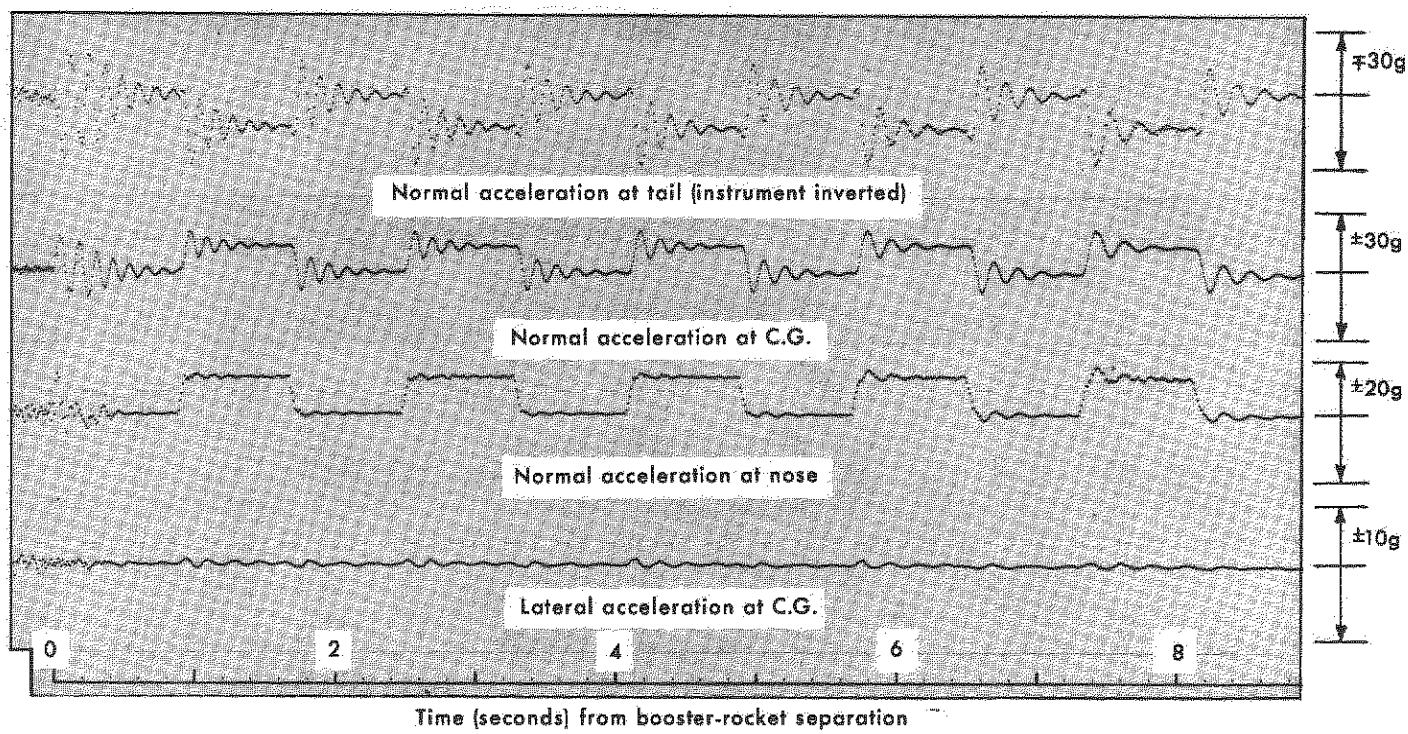

b. Model 3

Fig.11. Examples of flight records

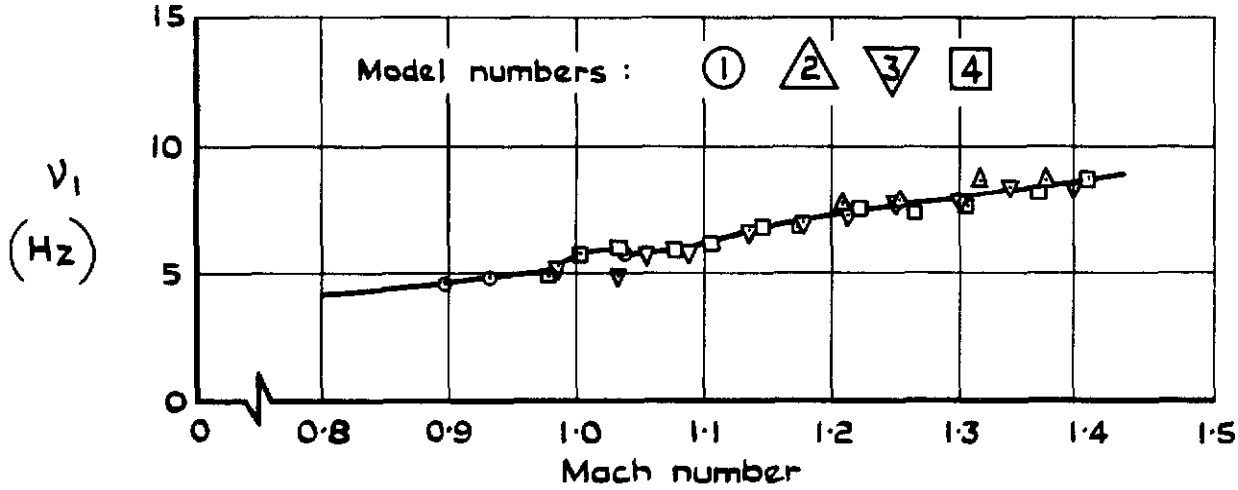

Fig. 12 Frequency of longitudinal short-period oscillation

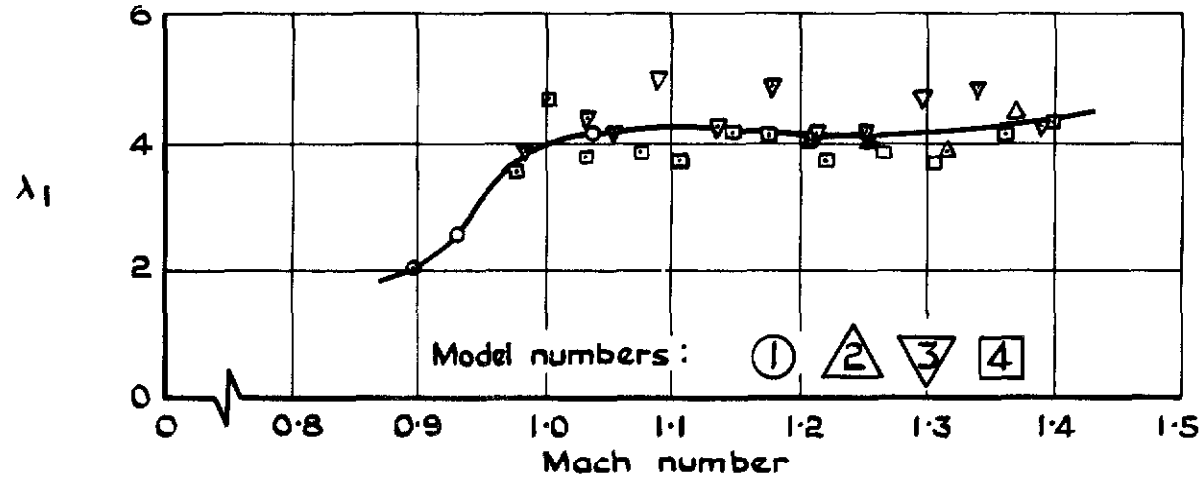

Fig. 13 Total damping of longitudinal short-period oscillation

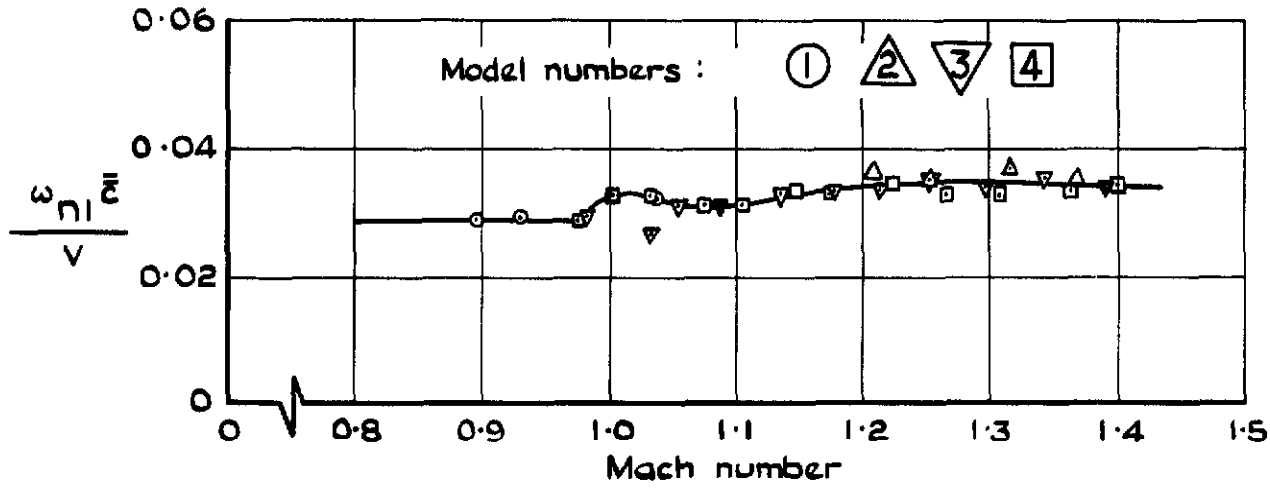

Fig. 14 Reduced undamped frequency of longitudinal short-period oscillation

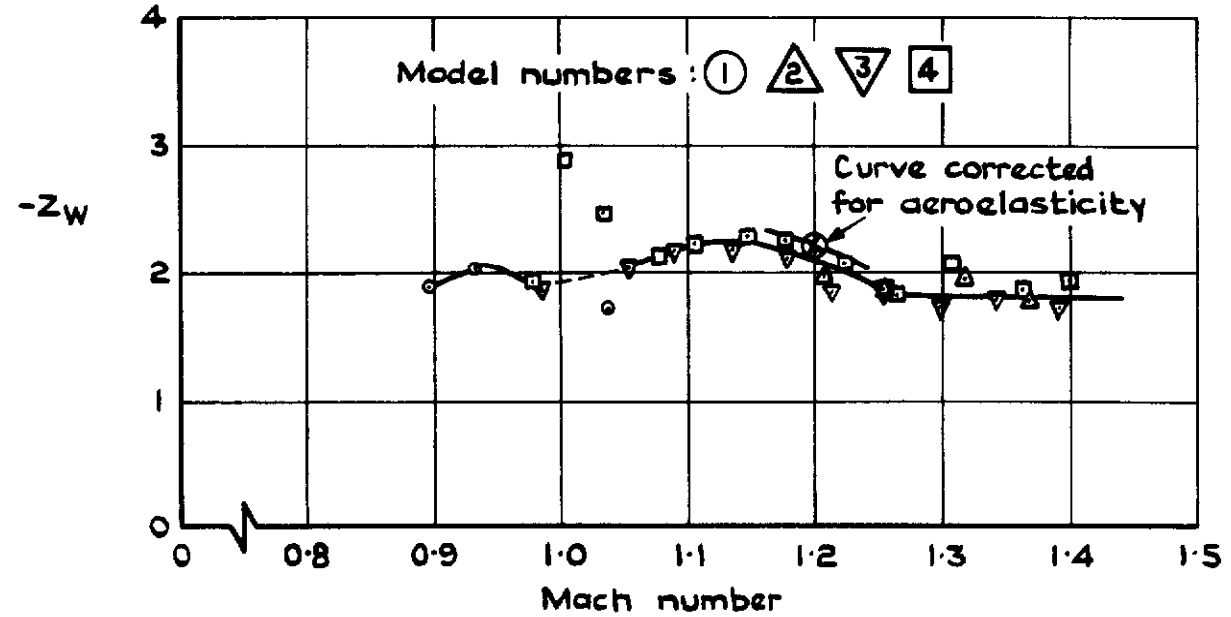

Fig.15 Normal-force derivative z_w

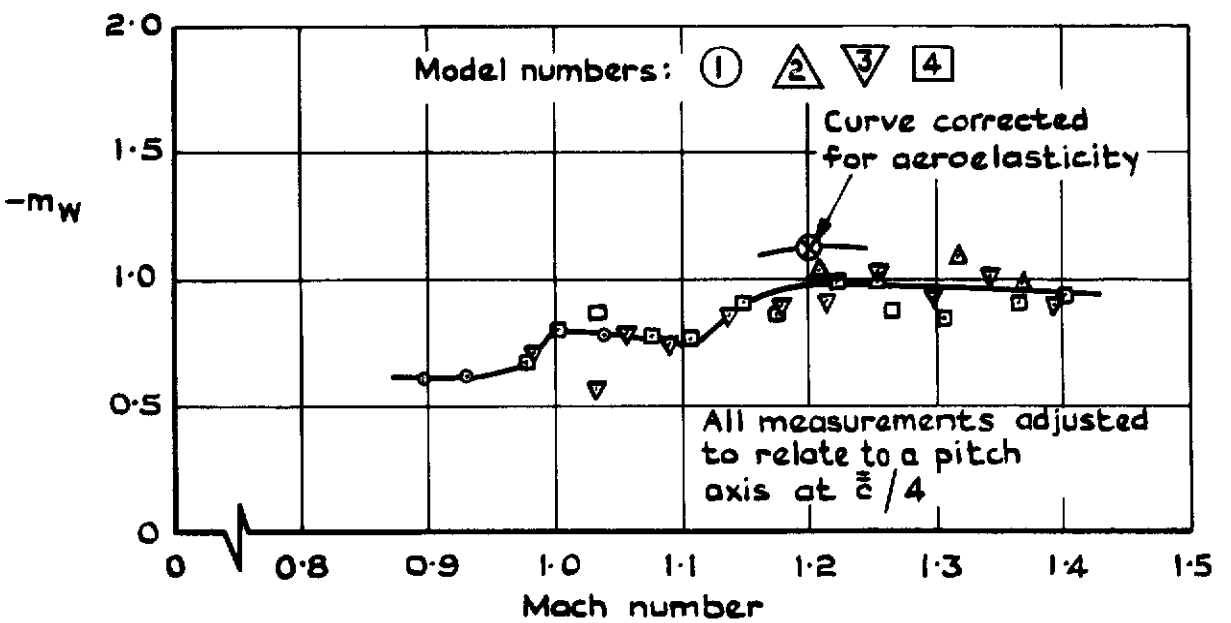

Fig.16 Pitching-moment derivative m_w

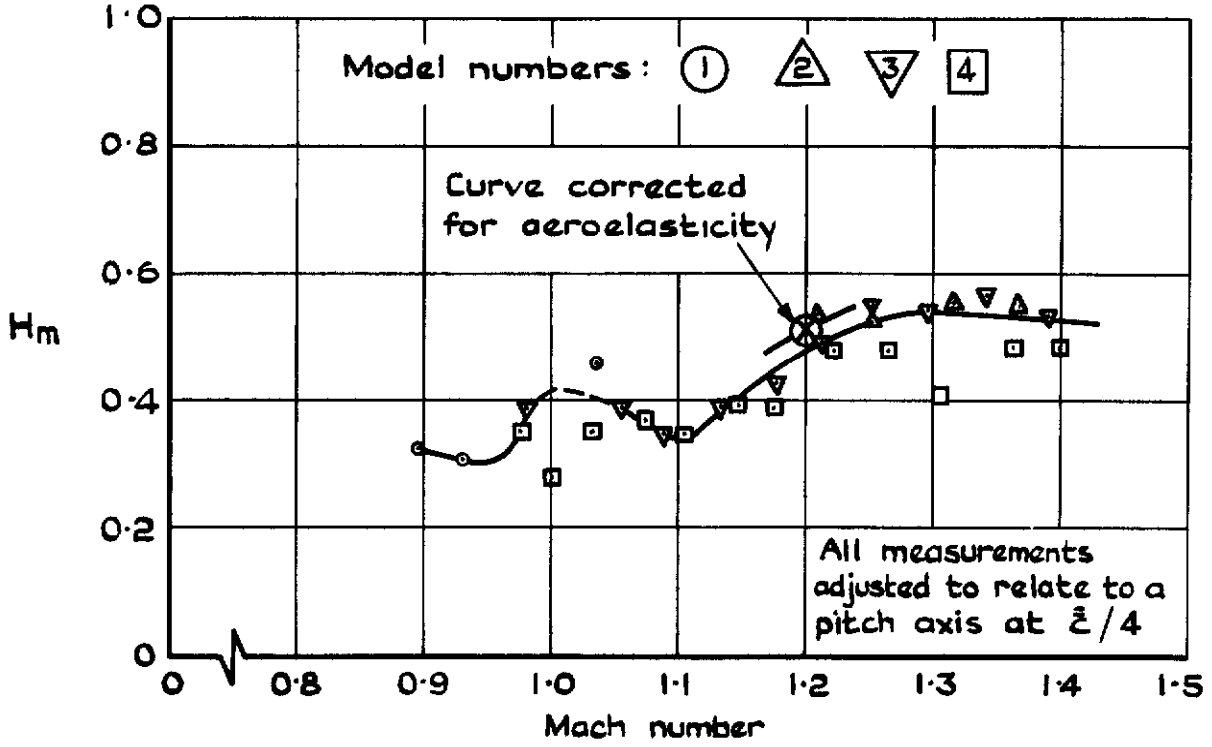

Fig. 17 Manoeuvre margin

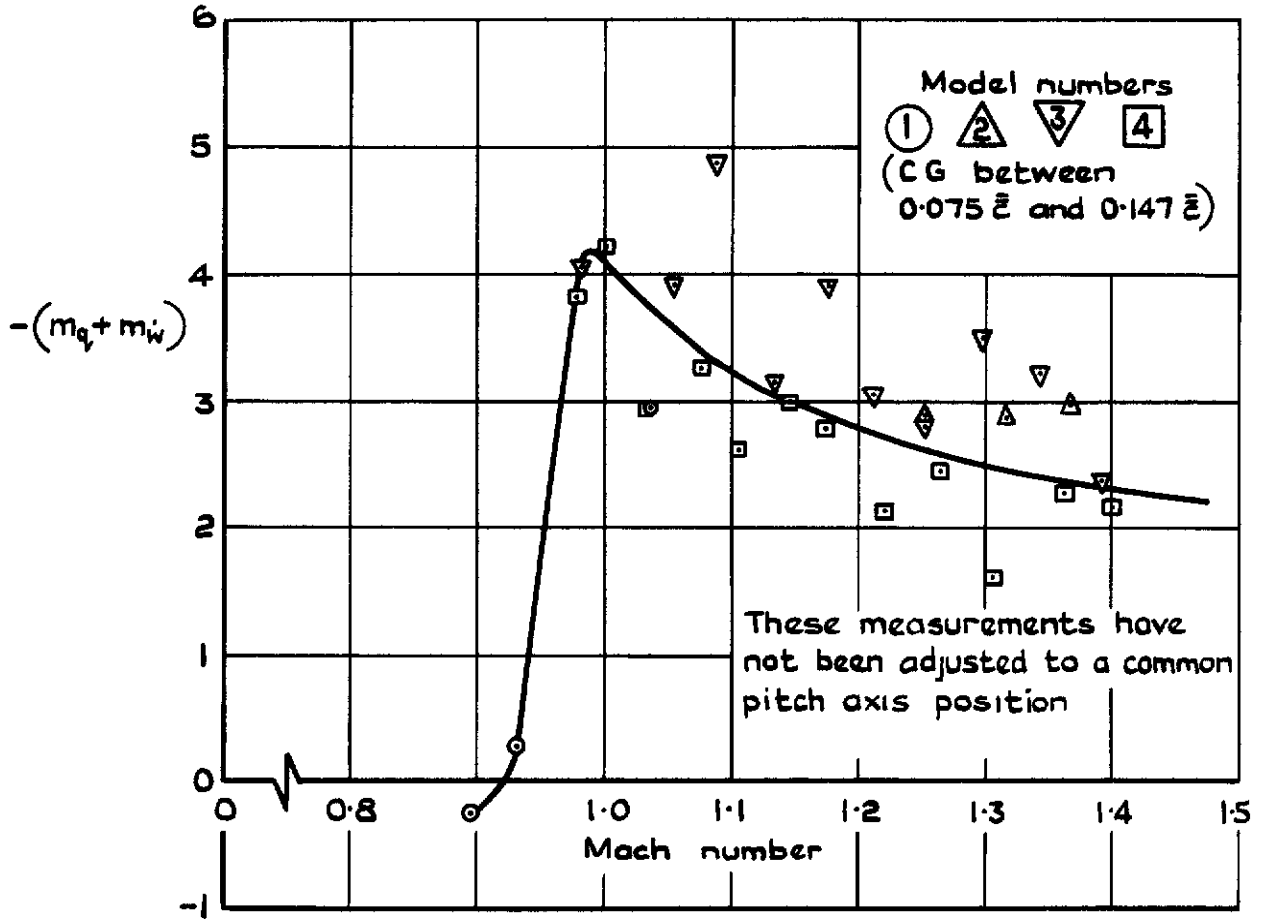

Fig. 18 Rotary damping in pitch $(m_q + m_{\dot{w}})$

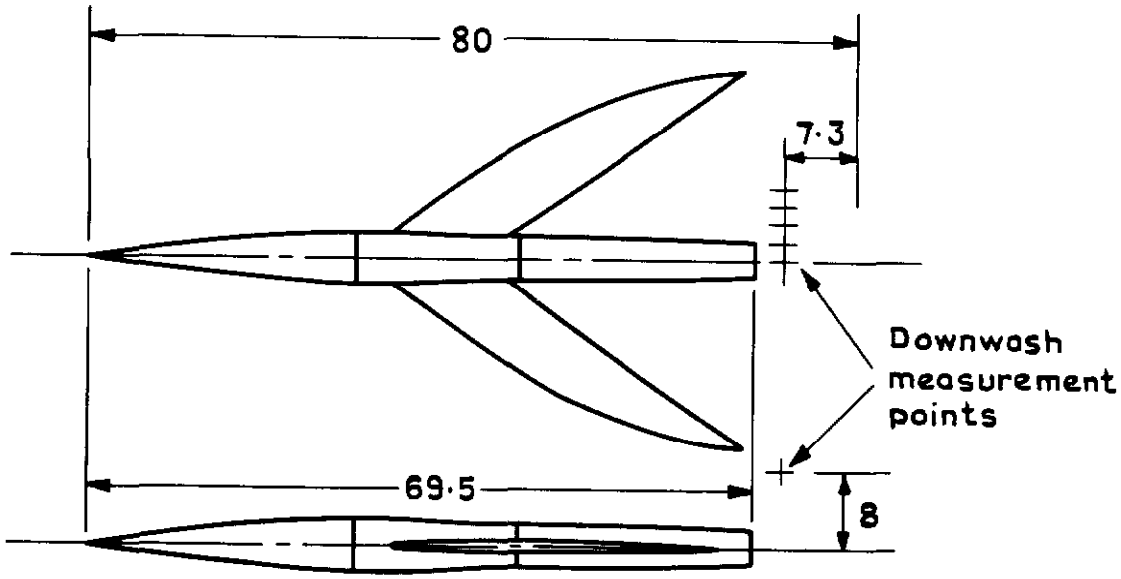

a Model 3

Dimensions in inches

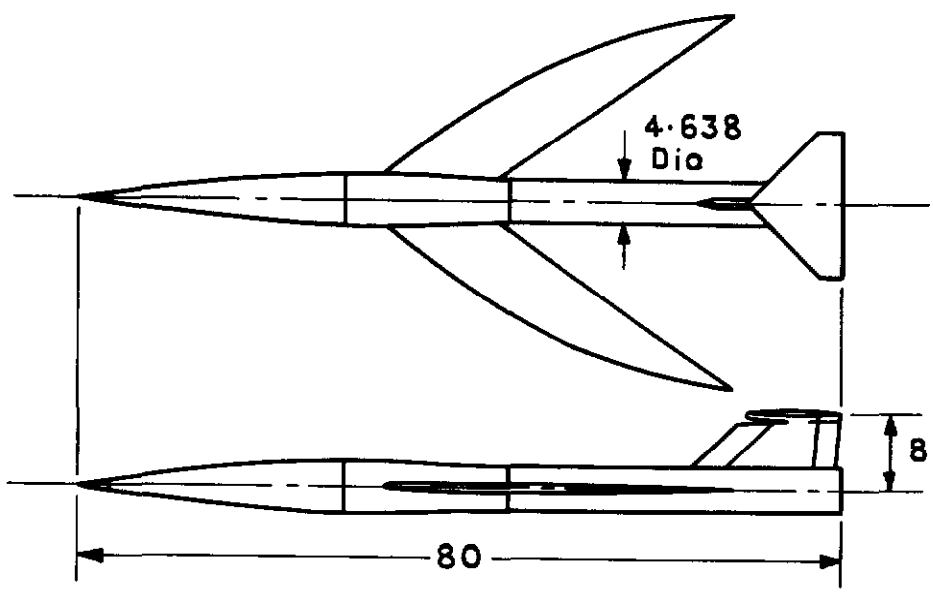

b Model 4

Fig. 19 Models 3 and 4 modified for wind-tunnel test

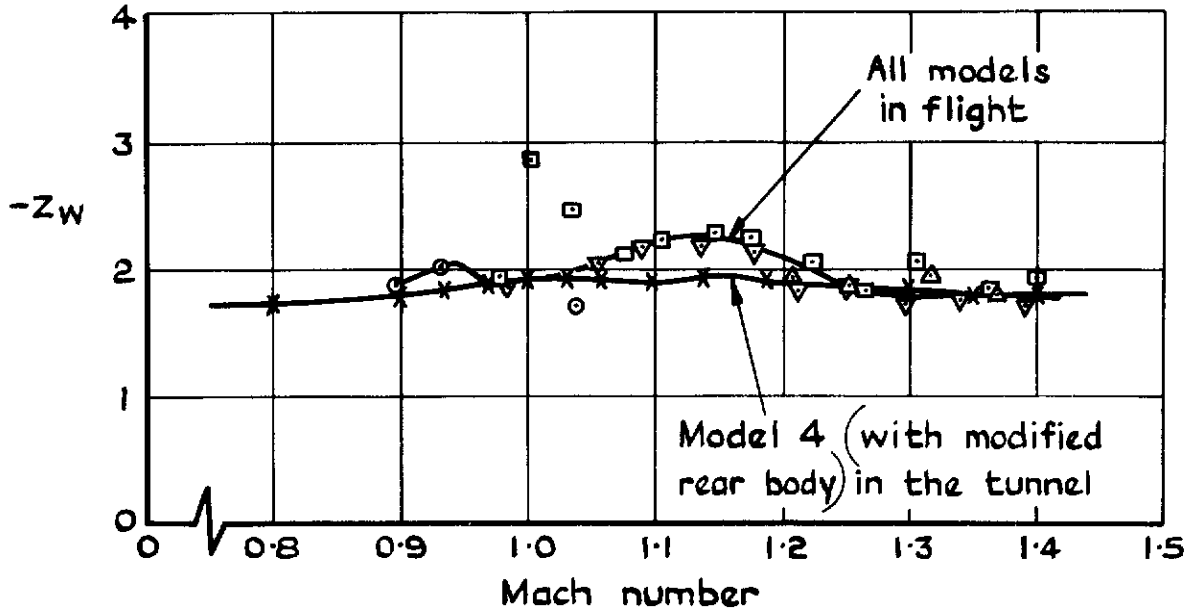

a Normal-force derivative z_w

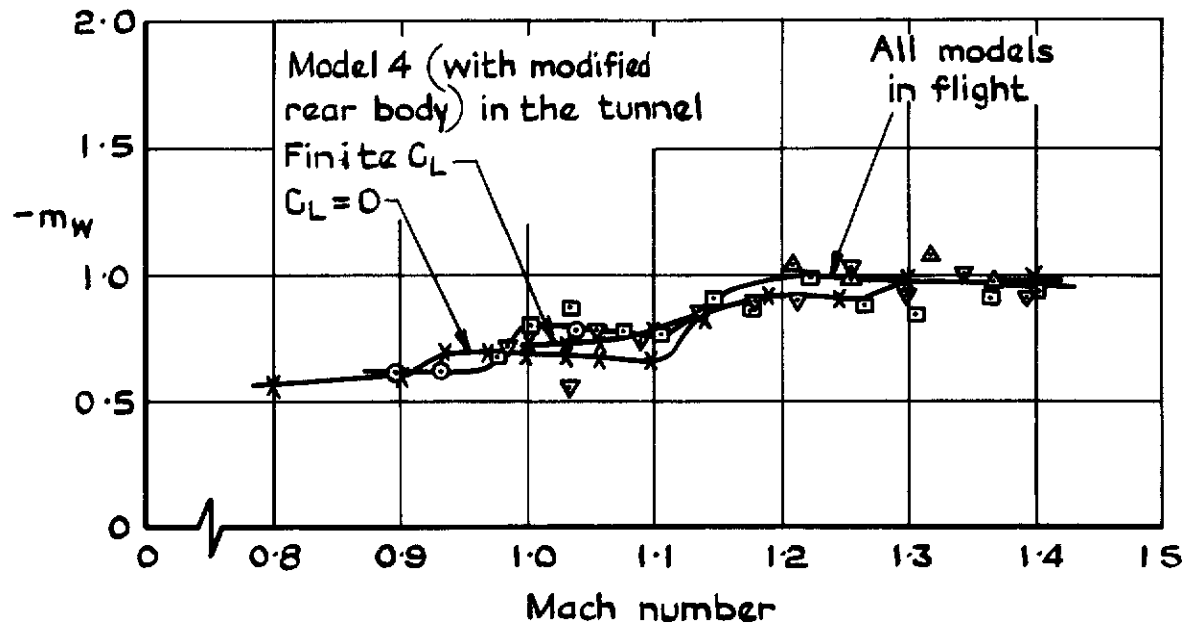

b Pitching-moment derivative m_w

Fig.20 Comparison between measurements made in free flight and in a wind tunnel (tail on)

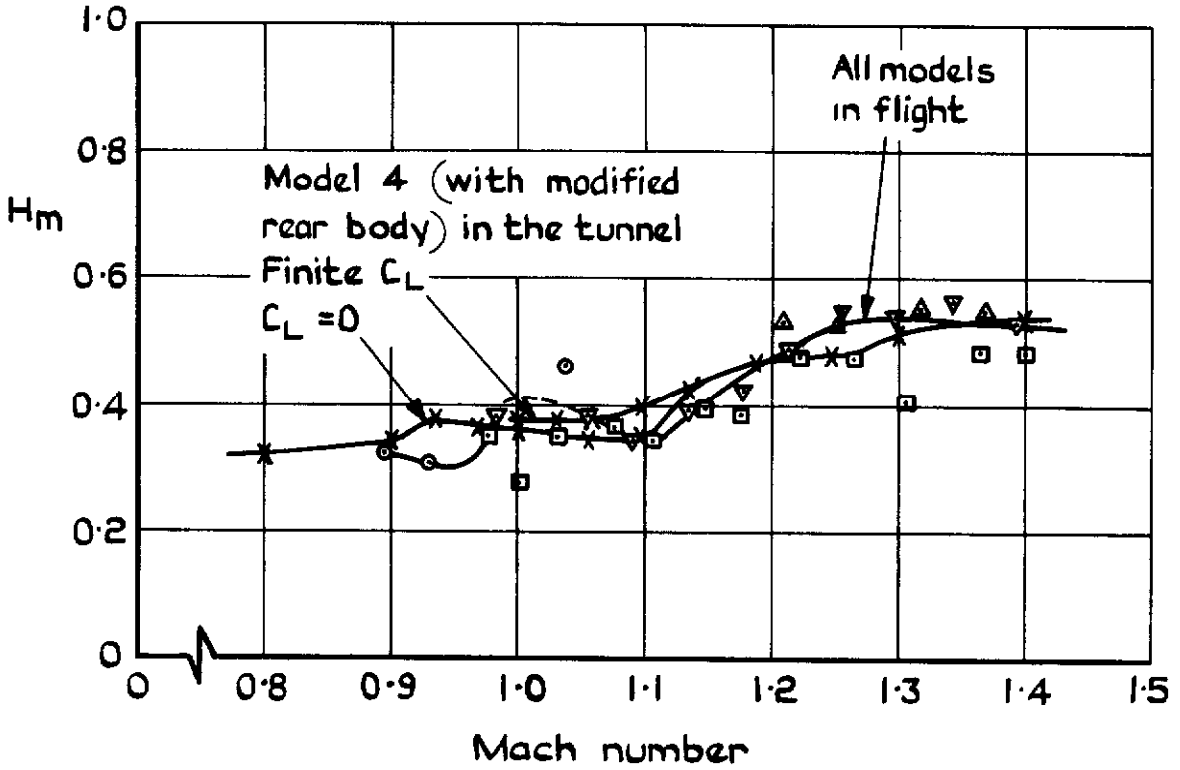

c Manoeuvre margin

Fig. 20 contd

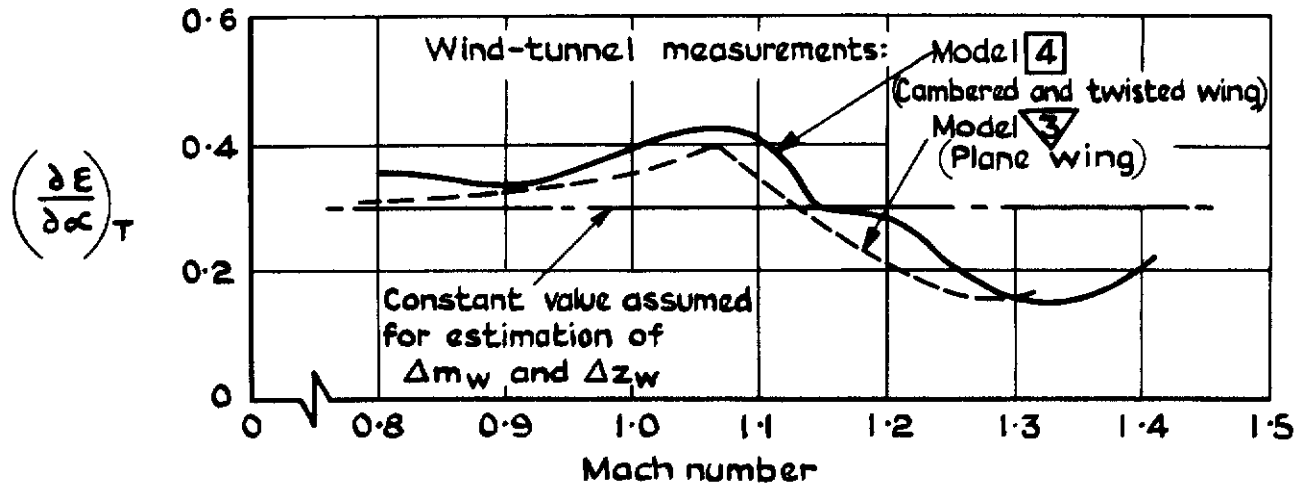

Fig. 21 Rate of change of downwash angle at the tail

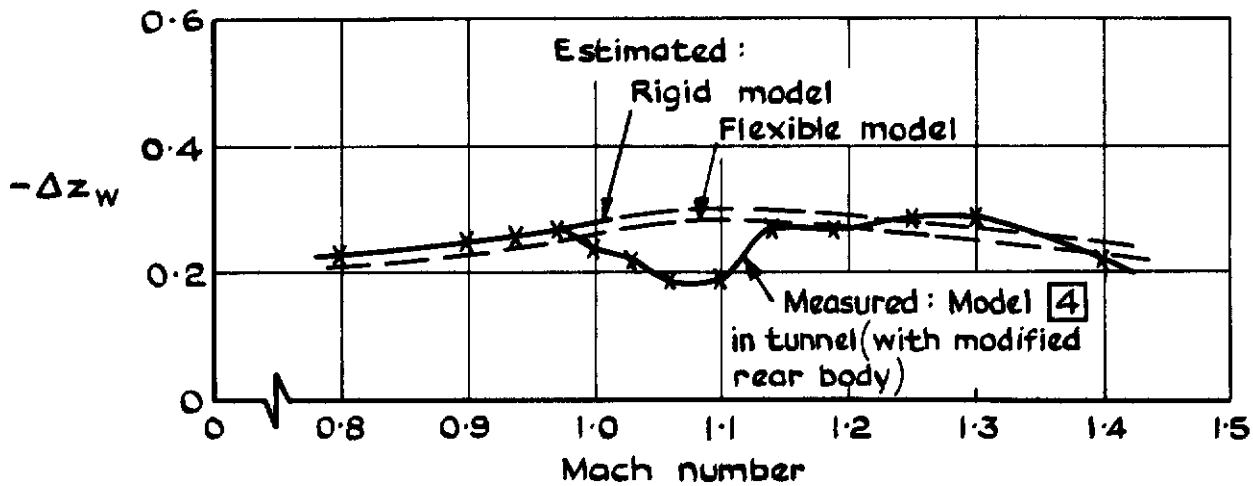

a Normal-force derivative z_w

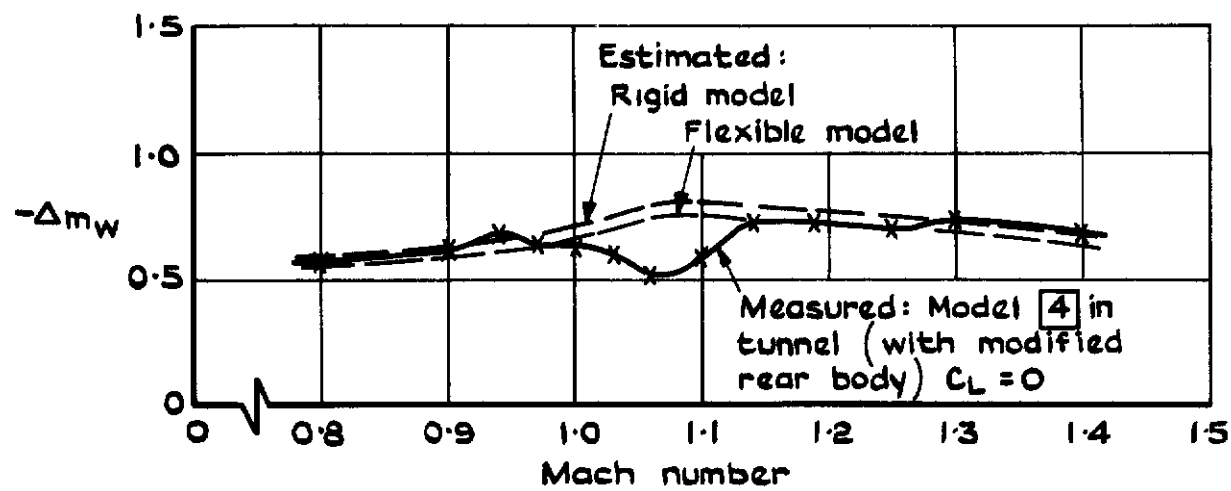

b Pitching moment derivative m_w

Fig. 22 Contributions from the tail to the derivatives z_w and m_w

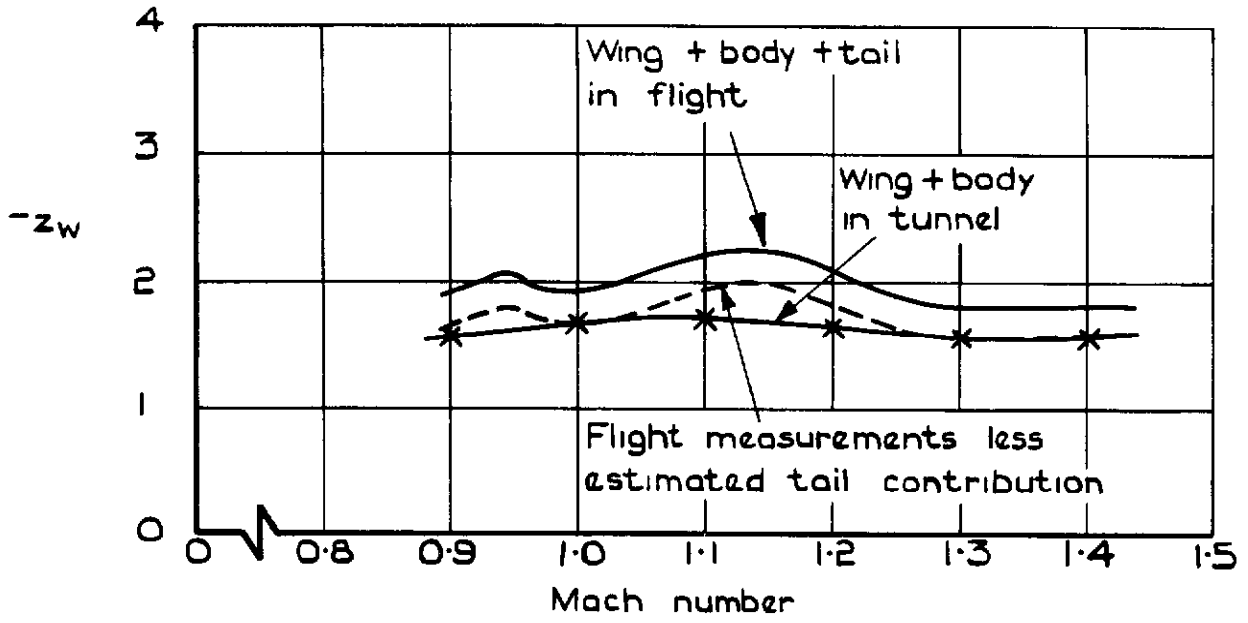

a Normal–force derivative z_w

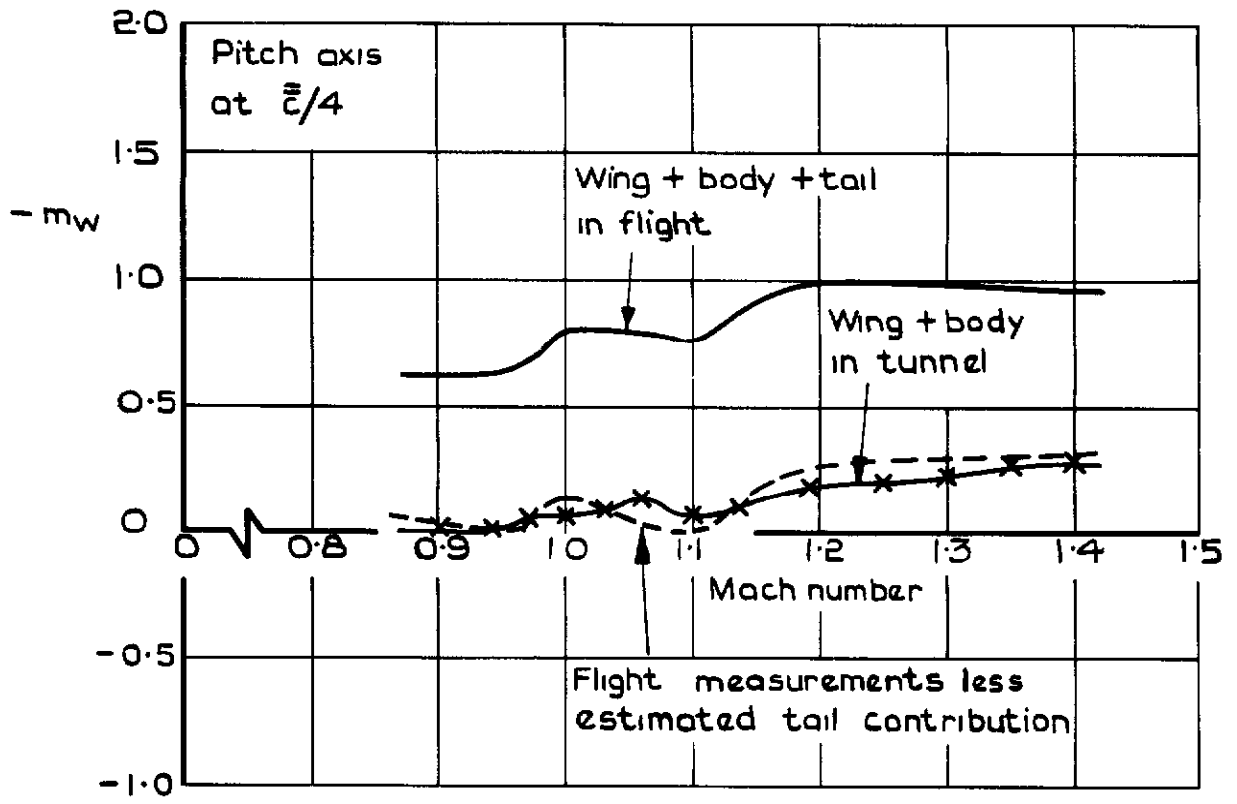

b Pitching–moment derivative m_w

Fig. 23 Static longitudinal stability characteristics of the wing–body combination

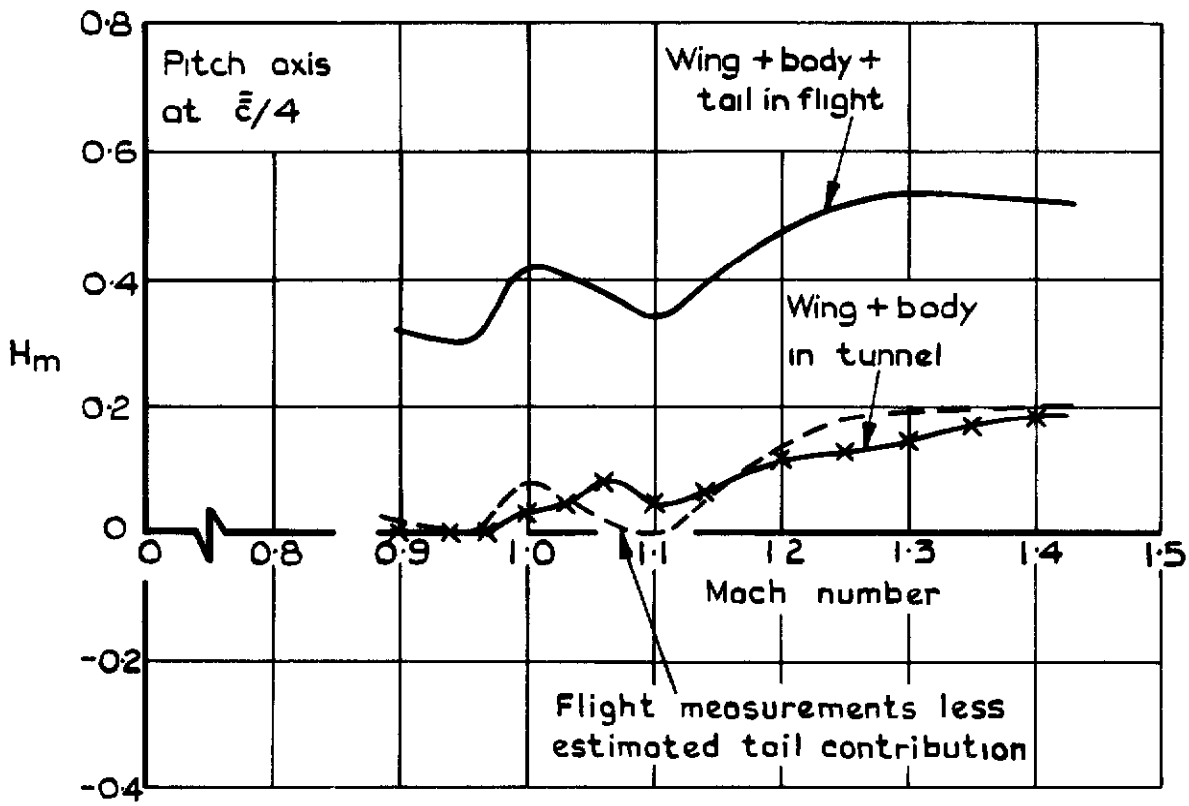

c Manoeuvre margin

Fig. 23 contd

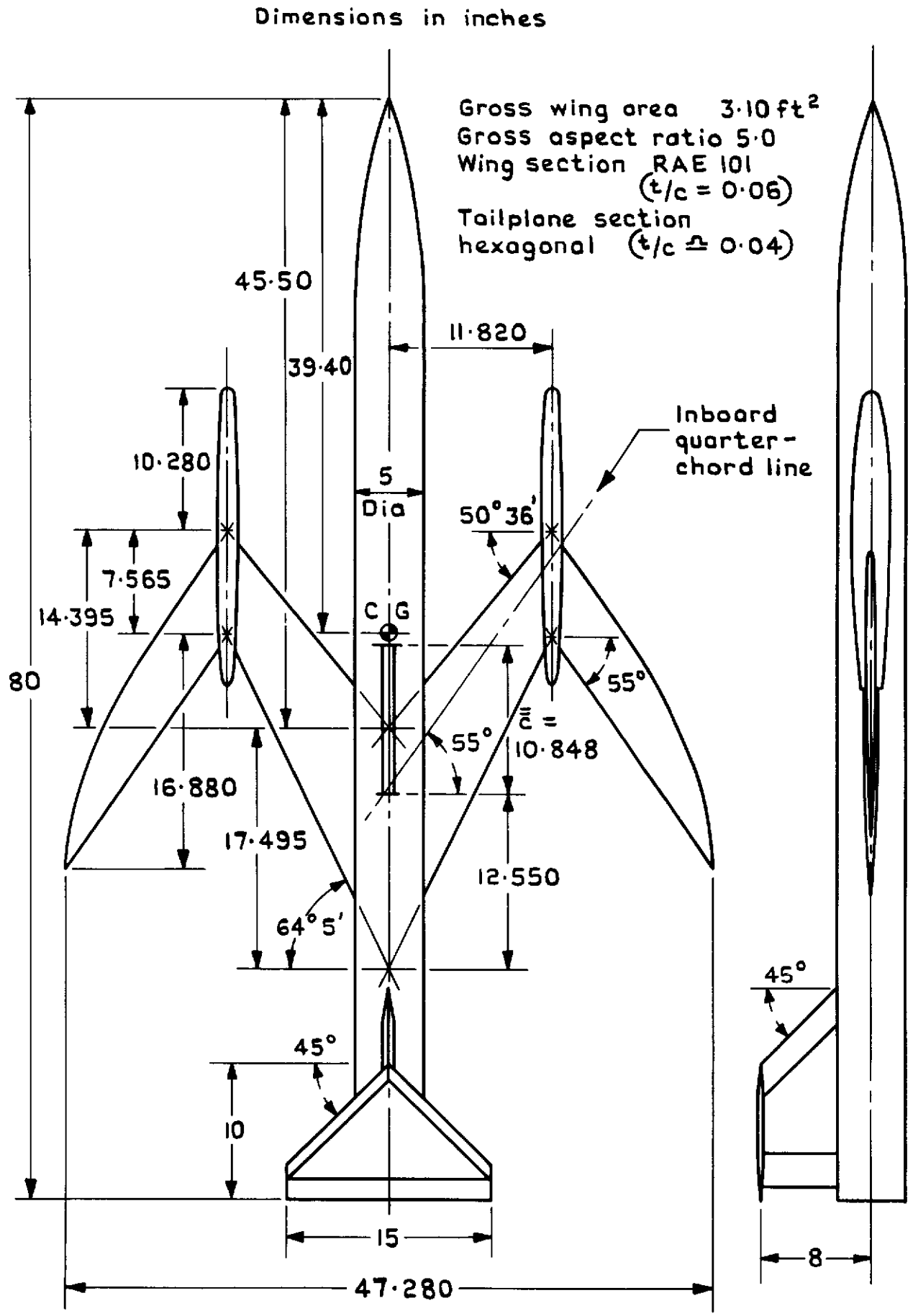

Fig. 24 The M-wing model (reference 10)

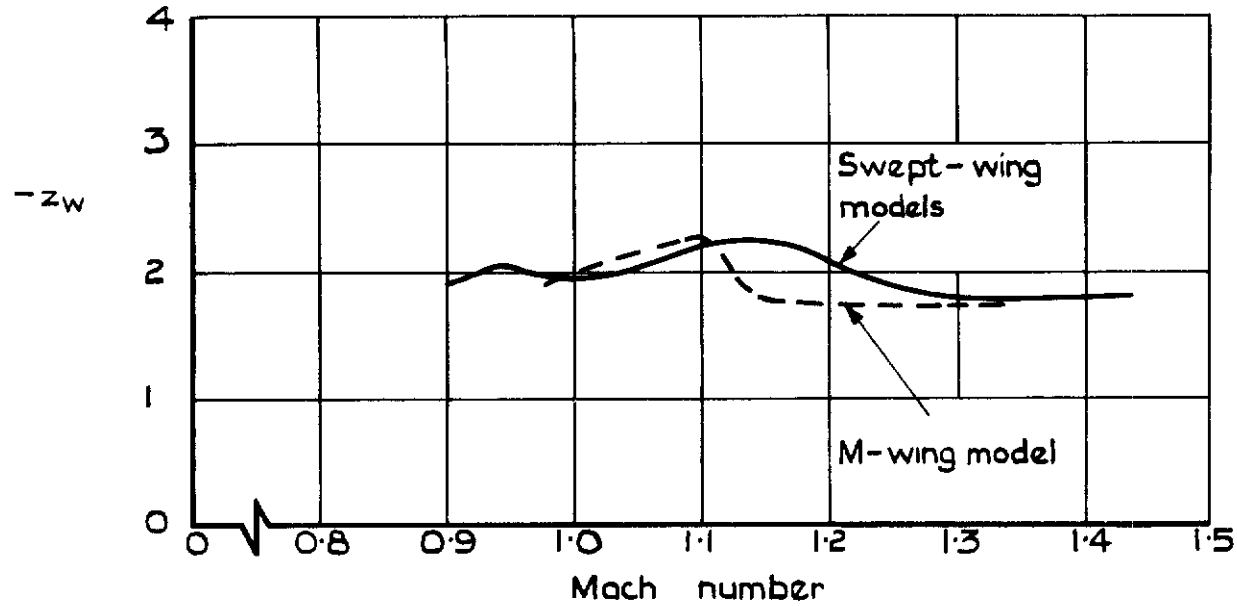

a Normal–force derivative z_w

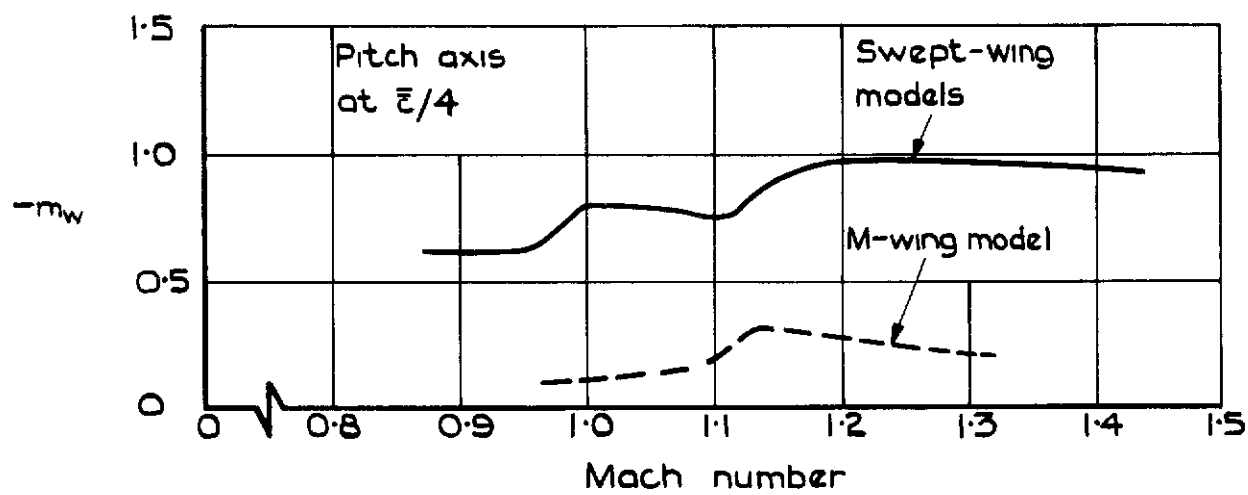

b Pitching–moment derivative m_w

Fig. 25 Longitudinal stability derivatives of swept–wing and M–wing models

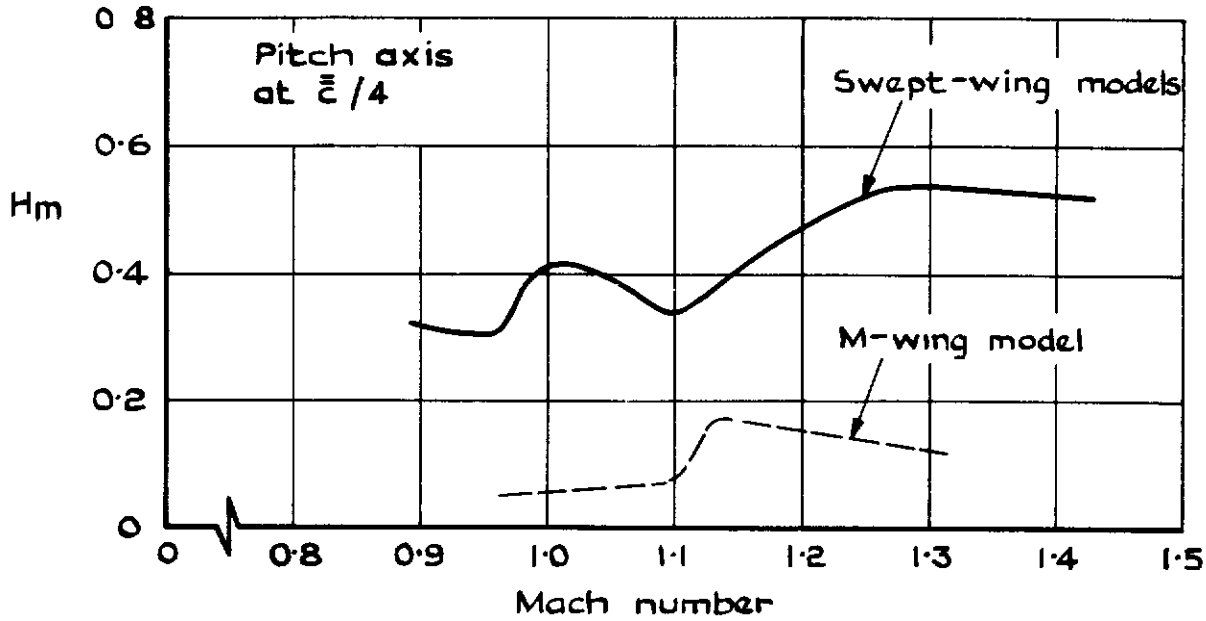

c Manoeuvre margin

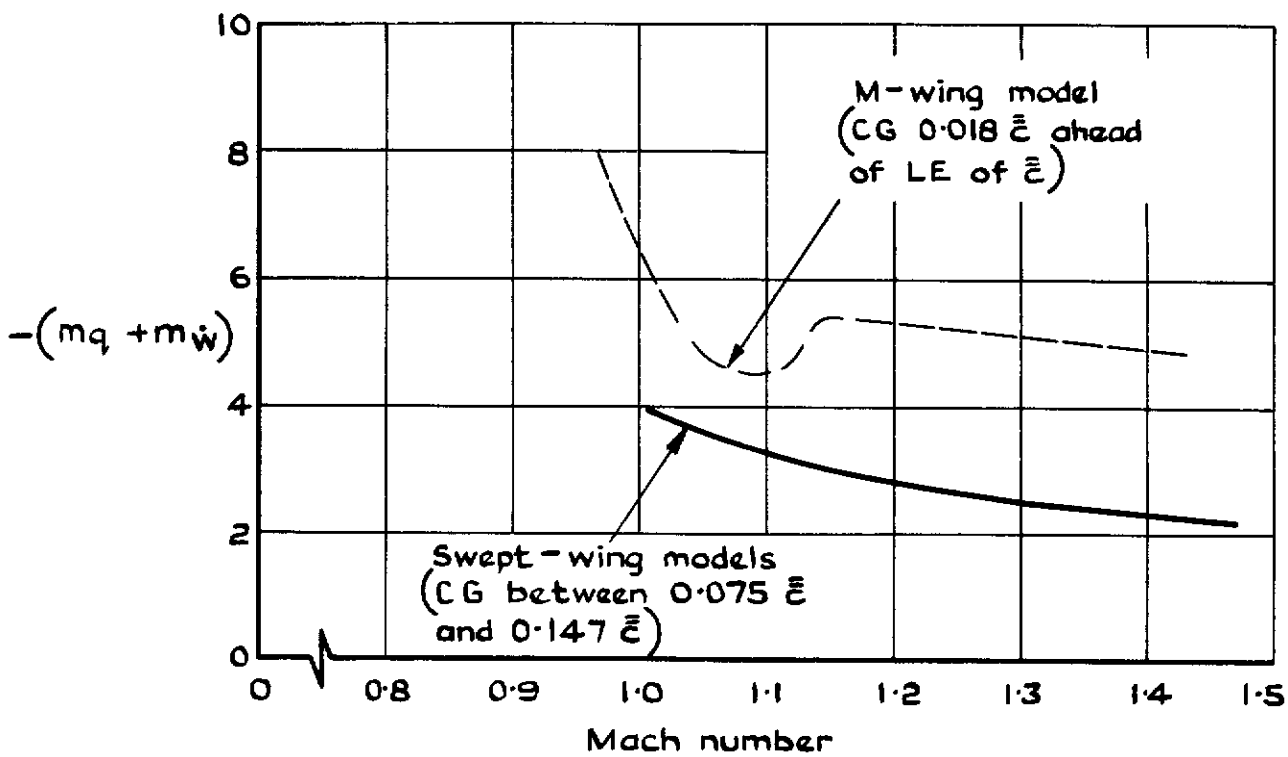

d Rotary damping in pitch $(m_q + m_{\dot{w}})$

Fig.25 contd

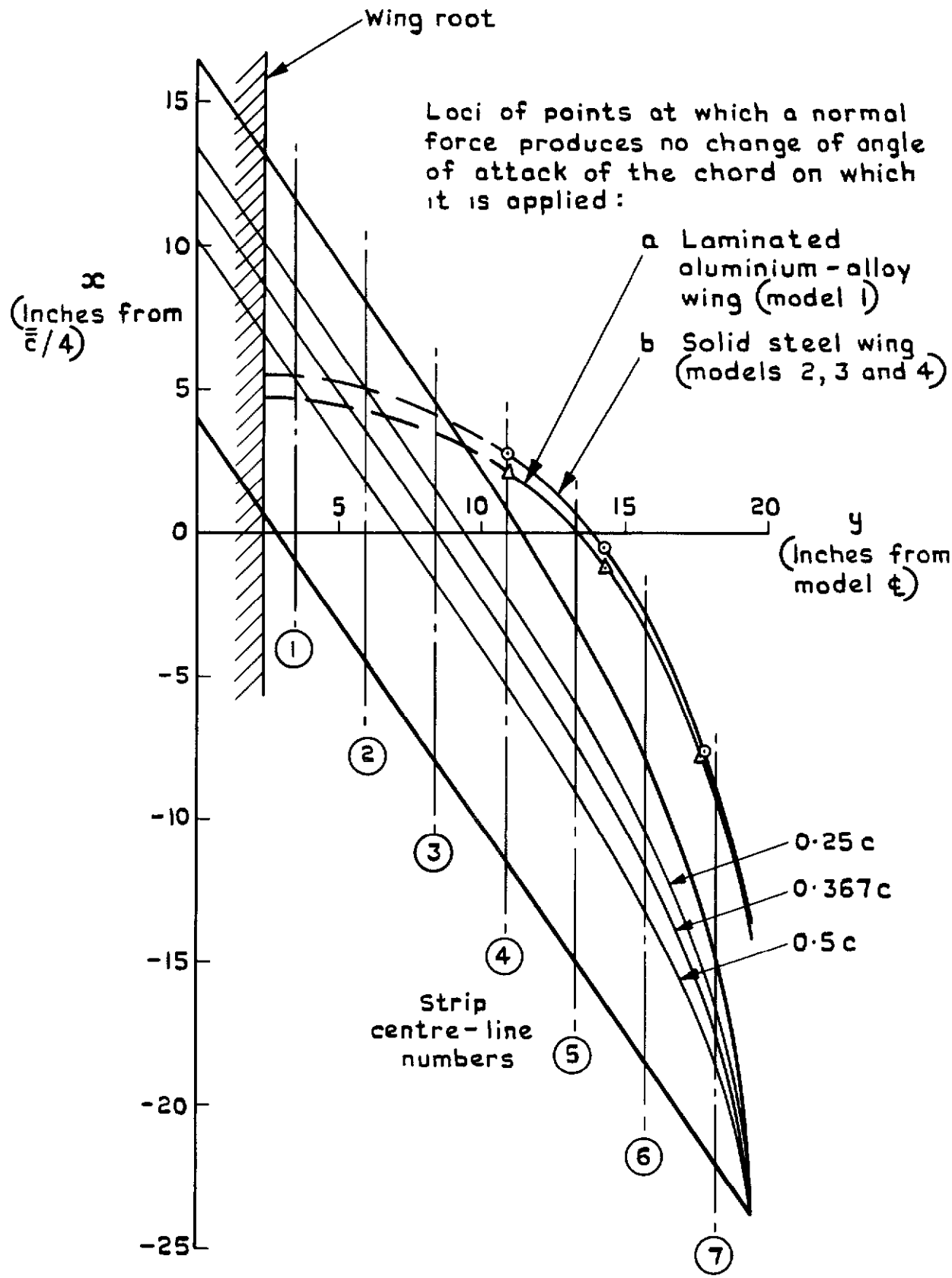

Fig. 26 Loading lines for determination of aeroelastic effects

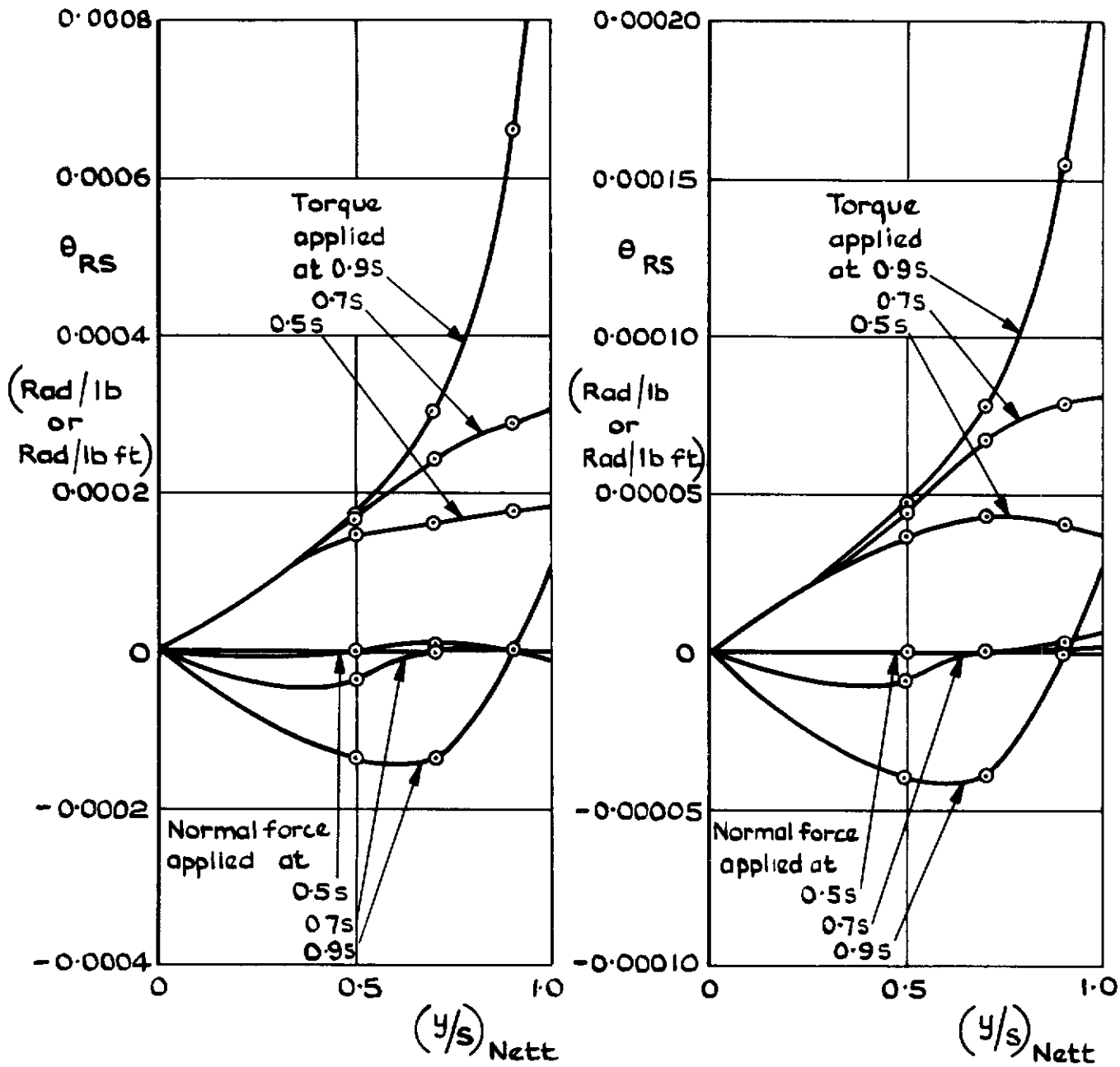

a Laminated aluminium alloy wing (model 1)

b Solid steel wing (models 2, 3 and 4)

Fig. 27 Change of local angle of attack caused by a unit load on the wing

Printed in England for Her Majesty's Stationery Office by the Royal Aircraft Establishment, Farnborough. Dd.146915. K.3.

A.R.C. C.P. No.1052
July 1968

Hunt, G.K.

533.6.055 :
533.6.013.412 :
629.137.1 :
533.6.011.35 :
533.693.1

FREE FLIGHT MODEL MEASUREMENTS OF THE LONGITUDINAL STABILITY OF A TRANSONIC SWEPT-WINGED AIRCRAFT

Four models of an aircraft configuration with a 55 degree swept wing were flown at Mach numbers between 0.9 and 1.4, at Reynolds numbers up to 10 million and lift coefficients between zero and 0.5. Measurements of the manoeuvre margin and the derivatives m_w, $(m_q + m_{\dot{w}})$ and z_w were obtained.

The results are compared with those obtained from one of the same models in a transonic wind tunnel and from a related M-wing model in flight. They are also corrected for aeroelastic effects.

A.R.C. C.P. No.1052
July 1968

Hunt, G.K.

533.6.055 :
533.6.013.412 :
629.137.1 :
533.6.011.35 :
533.693.1

FREE FLIGHT MODEL MEASUREMENTS OF THE LONGITUDINAL STABILITY OF A TRANSONIC SWEPT-WINGED AIRCRAFT

Four models of an aircraft configuration with a 55 degree swept wing were flown at Mach numbers between 0.9 and 1.4, at Reynolds numbers up to 10 million and lift coefficients between zero and 0.5. Measurements of the manoeuvre margin and the derivatives m_w, $(m_q + m_{\dot{w}})$ and z_w were obtained.

The results are compared with those obtained from one of the same models in a transonic wind tunnel and from a related M-wing model in flight. They are also corrected for aeroelastic effects.

A.R.C. C.P. No.1052
July 1968

Hunt, G.K.

533.6.055 :
533.6.013.412 :
629.137.1 :
533.6.011.35 :
533.693.1

FREE FLIGHT MODEL MEASUREMENTS OF THE LONGITUDINAL STABILITY OF A TRANSONIC SWEPT-WINGED AIRCRAFT

Four models of an aircraft configuration with a 55 degree swept wing were flown at Mach numbers between 0.9 and 1.4, at Reynolds numbers up to 10 million and lift coefficients between zero and 0.5. Measurements of the manoeuvre margin and the derivatives m_w, $(m_q + m_{\dot{w}})$ and z_w were obtained.

The results are compared with those obtained from one of the same models in a transonic wind tunnel and from a related M-wing model in flight. They are also corrected for aeroelastic effects.

DETACHABLE ABSTRACT CARDS

Published by
HER MAJESTY'S STATIONERY OFFICE

To be purchased from
49 High Holborn, London W C 1
13A Castle Street, Edinburgh 2
109 St Mary Street, Cardiff CF1 1JW
Brazennose Street, Manchester 2
50 Fairfax Street, Bristol BS1 3DE
258 Broad Street, Birmingham 1
7 Linenhall Street, Belfast BT2 8AY
or through any bookseller

C.P. No. 1052

SBN 11 470179 2